https://doi.org/10.5194/bg-2019-508
Preprint. Discussion started: 3 February 2020

Biogeosciences Discussions

Wide Discrepancies in the Magnitude and Direction of Modelled SIF in Response to Light Conditions

Nicholas C Parazoo[1], Troy Magney[1,2], Alex Norton[3], Brett Raczka[4], Cédric Bacour[5], Fabienne Maignan[6], Ian Baker[7], Yongguang Zhang[8], Bo Qiu[8], Mingjie Shi[9], Natasha MacBean[10], Dave R. Bowling[4], Sean P. Burns[11,12], Peter D. Blanken[11], Jochen Stutz[9], Katja Grossman[13], Christian Frankenberg[1,2]

Jet Propulsion Laboratory, California Institute of Technology[1]
California Institute of Technology[2]
School of Earth Sciences, University of Melbourne[3]
School of Biological Sciences, University of Utah[4]
NOVELTIS, 153 rue du Lac, 31670 Labège, France[5]
Laboratoire des Sciences du Climat et de l'Environnement, LSCE/IPSL[6]
Colorado State University[7]
International Institute for Earth System Sciences, Nanjing University, China[8]
University of California Los Angeles[9]
Department of Geography, Indiana University[10]
Department of Geography, University of Colorado[11]
National Center for Atmospheric Research[12]
Institute of Environmental Physics, University of Heidelberg[13]

Prepared for Biogeosciences

https://doi.org/10.5194/bg-2019-508
Preprint. Discussion started: 3 February 2020

Biogeosciences Discussions Open Access EGU

Abstract:

Recent successes in passive remote sensing of far-red solar induced chlorophyll fluorescence (SIF) have spurred development and integration of canopy-level fluorescence models in global terrestrial biosphere models (TBMs) for climate and carbon cycle research. The interaction of fluorescence with photochemistry at the leaf- and canopy- scale provides opportunities to diagnose and constrain model simulations of photosynthesis and related processes, through direct comparison to and assimilation of tower, airborne, and satellite data. TBMs describe key processes relating to absorption of sunlight, leaf-level fluorescence emission, scattering and reabsorption throughout the canopy. Here, we analyze simulations from an ensemble of process-based TBM-SIF models (SiB3, SiB4, CLM4.5, CLM5.0, BETHY, ORCHIDEE, BEPS) at a subalpine evergreen needleleaf forest near Niwot Ridge, Colorado. These models are forced with tower observed meteorological data, and analyzed against continuous far-red SIF and gross primary productivity (GPP) partitioned eddy covariance data at diurnal and synoptic scales during the growing season (July-August 2017). Our primary objective is to summarize the site-level state of the art in TBM-SIF modeling over a relatively short time period (summer) when light, structure, and pigments are similar, setting the stage for regional- to global-scale analyses. We find that these models are generally well constrained in simulating photosynthetic yield, but show strongly divergent patterns in the simulation of absorbed photosynthetic active radiation (PAR), absolute GPP and fluorescence, quantum yields, and light response at leaf and canopy scale. This study highlights the need for mechanistic modeling of non-photochemical quenching in stressed and unstressed environments, and improved representation of light absorption (APAR), distribution of sunlit and shaded light, and radiative transfer from leaf to canopy scale.

https://doi.org/10.5194/bg-2019-508
Preprint. Discussion started: 3 February 2020

Section 1: Introduction

Our ability to estimate and measure photosynthesis beyond the leaf scale is extremely limited. This inhibits the ability to evaluate the performance of terrestrial biosphere models (TBMs) that are designed to quantify the direct impact and feedbacks of the carbon cycle with climate change. Consequently, there are substantial uncertainties in estimating the gross primary production (GPP) response to environmental changes and carbon-climate feedback (Friedlingstein et al., 2014). Global, multi-scale remote sensing of solar induced fluorescence (SIF) may represent a major breakthrough in alleviating this deficiency (Mohammed et al, 2019). Spaceborne data indicate a linear relationship between SIF and GPP at large spatial (kilometer) and temporal (bi-weekly) scales (e.g., Sun et al., 2017) for several ecosystems, while ground-based measurements indicate a more non-linear relationship at leaf and canopy scales (Zhang et al., 2016; Gu et al., 2019; van der Tol et al., 2014; Magney et al., 2017, 2019a).

Chlorophyll fluorescence is re-emitted energy produced during the photosynthetic light reactions, in which a small fraction (roughly 2%) of photosynthetic active radiation (PAR) absorbed by chlorophyll is re-emitted at longer wavelengths (650-850 nm) as fluorescence. In ambient conditions, the emission of SIF represents a by-product of two primary de-excitation pathways, photochemical and nonphotochemical quenching (PQ, NPQ). Plants have evolved these regulatory mechanisms to prevent damage to photosynthetic machinery when the amount of absorbed radiation is greater than that which can be used to drive photochemistry. Chlorophyll fluorescence responds dynamically to changes in photochemistry and NPQ from instantaneous to hourly, daily, and seasonal timescales, as a function of changing environmental conditions and plant structural properties (Porcar-Castell et al., 2014; Demmig-Adams et al., 2012). SIF is fundamentally different than steady-state fluorescence yield typically measured at the leaf scale as it is sensitive to both changes in photochemistry as well as absorbed PAR (APAR, related to incident light, canopy structure, and biochemical content). The response of canopy SIF to APAR is well documented in deciduous and evergreen forests and cropping ecosystems (Yang et al., 2018; Badgley et al, 2017; Miao et al., 2018; Magney et al., 2019b; Li et al., 2020). More recently, Magney et al. (2019b) showed that seasonal changes in canopy SIF for cold climate evergreen

https://doi.org/10.5194/bg-2019-508
Preprint. Discussion started: 3 February 2020

77 systems is influenced by changes in needle physiology and photoprotective pigments (Magney et
78 al., 2019b).

79 To properly account for these factors, process-based SIF models must represent these underlying
80 non-linear biophysical and chemical processes. Several modeling groups have adapted TBMs to
81 incorporate various SIF formalisms for the purpose of model evaluation, data assimilation, and
82 improved model prediction (Lee et al., 2015; Koffi et al., 2015; Thum et al., 2017; Norton et al.,
83 2019; Bacour et al., 2019; Raczka et al., 2019). With these goals in mind, TBM SIF modeling
84 requires two important steps: (1) a representation of SIF at the needle/leaf scale that accounts
85 for NPQ and photochemistry, and (2) canopy radiative transfer of SIF, which enables a
86 comparison to large field-of-view observations (e.g. tower, satellites). The second step involves
87 accounting for radiative transfer within the canopy and has typically relied on incorporating the
88 Soil Canopy Observation Photosynthesis Energy model (SCOPE, van der Tol et al., 2009, 2014),
89 which simulates chlorophyll fluorescence as a function of biophysics, canopy structure,
90 environmental conditions, and sun/sensor geometries. This approach has been adopted by TBMs
91 in various ways using different assumptions for fluorescence modeling and radiative transfer, as
92 will be discussed in Section 2.

93 Typically, measuring chlorophyll fluorescence and competing pathways (PQ, NPQ) has been done
94 at the leaf scale via pulse-amplitude modulation fluorescence (PAM, Schreiber et al., 1986).
95 Recently, commercially available spectrometers have made it possible to measure SIF directly in
96 the field at the leaf and canopy scale, and also enable the study of structural, environmental, and
97 directional controls (Cogliati et al. 2015; Daumard et al. 2010; Migliavacca et al. 2017; Yang et al.
98 2015; Grossman et al., 2018; Gu et al., 2019b; Zhang et al., 2019). The use of field deployable
99 instruments on eddy covariance towers has increased rapidly since 2014, providing coverage of
100 multiple vegetation types across various climates around the world (Yang et al., 2018; Magney et
101 al., 2019a,b; Parazoo et al., 2019). These data enable improved understanding of the relationship
102 between SIF, GPP, APAR, and environmental effects at leaf to canopy scales. Novel tower-
103 mounted spectrometer systems such as Fluospec2 (Yang et al., 2018) and Photospec (Grossman
104 et al., 2018) have made it possible to monitor canopy SIF continuously in the field with high
105 precision over multiple years providing opportunities for more direct comparison and evaluation

https://doi.org/10.5194/bg-2019-508
Preprint. Discussion started: 3 February 2020

of satellite data (Grossman 2018; Yang 2015, 2018; Magney et al., 2019). PhotoSpec offers the additional benefits (and challenge) of (a) precise field of view capable of resolving leaf-level SIF, and (b) canopy scanning at azimuth and elevation angles. These features enable SIF integration from leaf- to canopy- scales, and interpretation of directional variations of the emitted radiance.

Canopy scanning spectrometers such as PhotoSpec thus provide an opportunity to understand the physical processes that lead to a breakdown of SIF-GPP linearity at leaf to canopy scale (or conversely, emergence of linearity at increasing scale), and for detailed evaluation and diagnosis of TBM performance. This study provides a preliminary benchmarking site-level assessment for simulations of SIF within a TBM framework and across an ensemble of TBMs, with the primary purpose being an initial investigation into the response of modelled SIF and GPP to light during peak summer. We leverage continuous measurements of SIF and GPP at the Niwot Ridge US-NR1 Ameriflux flux tower in Colorado from June-July 2017 (Magney et al., 2019b) to (1) Benchmark TBM-SIF modeling, (2) Evaluate sensitivity to underlying processes and scaling techniques, (3) Identify strengths and weaknesses in current modeling strategies, and (4) Recommend strategies for models and observations.

The paper is organized as follows: Section 2 describes the seven TBM-SIF models (SiB3, SiB4, ORCHIDEE, BEPS, BETHY, CLM4.5, CLM5) which have recently been published or are in review, and provides more details on site level benchmarking observations. Section 3 summarizes results comparing modelled and predicted SIF and GPP at hourly and daily scales, as they relate to absorbed light, GPP and SIF yields, and quantum yields. Section 4 discusses results in more detail, including attribution of SIF magnitude and temporal phasing biases and sensitivities to absorbed light, and areas for improvement.

Section 2: Methods

2.1 Site: Niwot Ridge, Colorado

Our study focuses on an AmeriFlux (https://ameriflux.lbl.gov/) site in Niwot Ridge, Colorado, USA (US-NR1), where a tower-based eddy covariance system has been continuously measuring the net ecosystem exchange of carbon dioxide (NEE) over a high-elevation subalpine forest since 1999, and a spectrometer system that has been continuously monitoring SIF since June

https://doi.org/10.5194/bg-2019-508
Preprint. Discussion started: 3 February 2020

2017 (Grossman et al., 2018; Magney et al., 2019b). The 26-m tall tower is located in a high elevation forest (3050 m asl) located in the Rocky Mountains of Colorado (Burns et al., 2015; Hu et al., 2010; Monson et al., 2002) and consists primarily of the evergreen species of lodgepole pine (*Pinus contorta*), Engelmann spruce (*Piceae engelmanii*), and subalpine fir (*Abies lasiocarpa*). The mean annual temperature is 1.5°C and mean annual precipitation is 800 mm (65% as snow). The forest is roughly 120 years old with a mean canopy height of 11.5 m, and a leaf area index of 4.2 m^2 m^{-2}. More site-specific details can be found in Burns et al. (2015).

At Niwot Ridge, interannual variations in GPP are closely linked to winter snowfall amount, which typically melts by early June, and summer precipitation, characterized by afternoon convective thunderstorms triggered by upslope flow (Burns et al., 2015; Albert et al., 2017) and climatological peak precipitation around 2 pm local time (Fig 1A). We note that our study period of July-August 2017 is unusual for NR1 (relative to the 2015-2018 mean) in its bimodal distribution of diurnal precipitation (morning and afternoon peaks), lower than normal afternoon precipitation, cooler temperatures, and reduced vapor pressure deficit (Fig 1 A-C). The early morning peak is due to a strong storm system that moved through from July 22-24 (Fig 1E), and does not show up when these days are removed. This period also shows a decrease in incoming shortwave relative to climatology despite lower precipitation (Fig 1D). We note that a second storm passed through in early August. The combination of these two storms produced net decreases in air temperature (Fig 1F), vapor pressure deficit (Fig 1G) and sunlight (Fig 1H) over a two-week period from late July to early August.

2.2 Tower-Based Measurements: PAR, SIF, CO_2 Flux

2.2.1 Absorbed PAR

The site is equipped with two main upward-facing PAR sensors. The first (LICOR LI-190R), mounted on the PhotoSpec telescope unit, provides an independent measurement of direct/diffuse light and can be used to calibrate PhotoSpec (Grossman et al., 2018). The second (SQ-500-SS; Apogee Instruments), mounted on the main flux tower, is part of a larger array of upward- and downward-oriented PAR sensors above and below the canopy used for the calculation of the fraction of PAR absorbed by the vegetation canopy (fAPAR). The two PAR

https://doi.org/10.5194/bg-2019-508
Preprint. Discussion started: 3 February 2020

sensors show a similar diurnal pattern during July-August 2017 (Fig S1), including an afternoon dip and relatively smaller values overall compared to 2018 (the only other year with available PAR for comparison).

Full-spectrum quantum sensors (SQ-500-SS; Apogee Instruments) were new and factory-calibrated together just before installation. Above-canopy sensors (one up and one down-facing) were mounted on the main flux tower, and below-canopy sensors (six up and six down) were mounted at the 2 m height above ground on a shorter canopy-access towers. APAR was calculated for each pair of below-canopy relative to above-canopy sensors for every half-hour, then averaged among sensors over daylight hours to create a daytime average. We then estimate hourly APAR by multiplying hourly incoming PAR (measured and integrated from 400-700 nm) at the top of canopy (PAR) by the daytime average of fAPAR. Fig S2 shows the mean diurnal cycle for July-August 2017 for each sensor, and the across-sensor average, with APAR data collection beginning on July 13, 2017.

2.2.2 Tower Based Measurements of Solar Induced Chlorophyll Fluorescence (SIF)

SIF data has been collected from a scanning spectrometer (PhotoSpec) installed at the AmeriFlux US-NR1 tall tower since June 17, 2017. PhotoSpec sits atop the tower at 26 m above the ground and roughly 15 m above the forest canopy top, transferring reflected sunlight and SIF data collected from the needleleaf canopy through a tri-furcated optical cable to three spectrometers in a shed at the base of the tower. These spectrometers measure far-red fluorescence in the 745-758 nm retrieval window at high spectral resolution (FWHM = 0.3 nm) and with a 0.7 deg field of view (FOV), resulting in a 20-cm diameter footprint at nadir on top of the canopy. The far-red SIF data are then scaled to 740 nm for model intercomparison using the first principal component of the spectral shape in Magney et al., 2019a. Photospec scans from nadir to the horizon in 0.7 degrees steps at two azimuth directions, with a time resolution of ~20 s per measurement and complete scan time of 20 minutes. For this study, we aggregate scans across all azimuth and elevation angles into hourly, canopy level averages to benchmark model estimates of top of canopy (TOC) or canopy averaged SIF (BETHY only, see Sec *2.3.4.*1) at diurnal and synoptic time scales. We refer the reader to Grossman et al. (2018) and Magney et al (2019b) for further details

https://doi.org/10.5194/bg-2019-508
Preprint. Discussion started: 3 February 2020

regarding PhotoSpec, implementation at US-NR1, and data filtering. A two-month data collection gap in fall of 2017 limits our model-data analysis to the 2017 growing season (July-August, 2017).

Diurnal composites of PhotoSpec SIF in 2017 show a late morning peak and afternoon dip (Fig S3A). The afternoon dip is consistent with decreased incoming shortwave, PAR and APAR (Figs S1 and S2, respectively). However, we note the retrieved signal from PhotoSpec is also affected by (1) viewing geometry, (2) fraction of sunlit vs shaded leaves (sun/shade fraction, i.e. the quantity of needles illuminated by incident sunlight) due to self-shading within the canopy, and (3) direct/diffuse fraction due to cloud cover. Structural and bidirectional effects lead to different SIF emission patterns depending on view angle and scanning patterns (Yang and van der Tol, 2018). The viewing geometry of PhotoSpec (as implemented at NR1 in 2017) causes a higher fraction of illuminated vegetation in the morning, which leads to a 2 to 3 hour offset in the timing of peak SIF (Fig S3A) and incoming far-red reflected radiance within the retrieval window (Fig S3B), from the peak zenith angle of the sun at noon (coinciding with the expected peak in PAR) to late morning. Normalizing SIF by far-red reflected radiance as relative SIF (SIF_{rel}, Fig S3C) and rescaling to SIF (Fig S3D) shifts the peak back to noon and preserved the afternoon dip (albeit with reduced magnitude). SIF_{rel} helps to account for factors 1-3 listed above because it accounts for the amount of reflected radiation in the field of view of PhotoSpec, which is impacted by canopy structure, sun angle, and direct/diffuse light. SIF_{rel} is likely a better approximation of SIF_{yield} because we are normalizing for the exact amount of 'illuminated' canopy elements in each retrieval, whereas the APAR measurements are integrated for the entire canopy. As such, we expect SIF_{rel} to have a strong seasonal change associated with downregulation of photosynthesis, and a more subtle diurnal change, as during mid-summer the SIF signal is primarily driven by light intensity.

It is important to note that the PhotoSpec system is highly sensitive to sun/shade fraction in the canopy (factor 2) due to the narrow FOV of the PhotoSpec telescoping lens. Increased afternoon cloud cover during summer causes diurnal asymmetry in incident PAR (Fig S1A). We examine this effect in more detail (Section 3) by analyzing SIF and GPP under clear and diffuse sky conditions using a threshold (0.5, top-of-canopy/top-of-atmosphere incoming shortwave radiation) similar to that used in Yang et al. (2017) and Yang et al. (2018).

https://doi.org/10.5194/bg-2019-508
Preprint. Discussion started: 3 February 2020

219 2.2.3 CO_2 Flux and GPP Partitioning

220 NEE measurements are screened using u_{star} filtering, and partitioned into gross primary
221 production (GPP) and terrestrial ecosystem respiration components using the so-called nighttime
222 method which is based on the relationship between NEE during the nighttime (PAR < 50 umol m^{-2}
223 s^{-1}) and air temperature (Reichstein et al., 2005). Diurnal averages of GPP based on nighttime
224 partitioning show similar diurnal structure to PAR and SIF including the afternoon dip and
225 reduced overall magnitude compared to the 2015-2018 mean (Fig S4). Similar results are found
226 using daytime light partitioning of NEE (Lasslop et al., 2010; Fig S4) and thus only nighttime
227 partitioned GPP data are reported for the remainder of this study. All GPP estimates are
228 processed as half hourly means, then gap filled and averaged hourly. Details on the flux
229 measurements, data processing and quality control are provided in Burns et al. (2015).

230 2.3 Modeling Approach

231 *2.3.1 TBM-SIF Overview*

232 The parent TBMs are designed to simulate the exchanges of carbon, water, and energy between
233 biosphere and atmosphere, from global to local scales depending on inputs from meteorological
234 forcing, soil texture, and plant functional type. The addition of a fluorescence model that
235 simulates SIF enables a direct comparison to remotely sensed observations for benchmarking,
236 process diagnostics, and parameter/state optimization (data fusion) for improved GPP
237 estimation. The TBM-SIF models analyzed here differ in ways too numerous to discuss. We refer
238 the reader to the appropriate references in Section 2.3.4 for more detailed model descriptions.
239 Instead, we focus on key differences affecting joint simulation of GPP and leaf/canopy level SIF
240 at diurnal and synoptic scale, during the peak of summer. These differences, which are
241 summarized in Table 1, include the representation of stomatal-conductance (all use Ball-Berry
242 except CLM5.0, BEPS, and ORCHIDEE), canopy absorption of incoming radiation, limiting factors
243 for photosynthesis (Vcmax, LAI, radiation, stress) and SIF (k_N), scaling and radiative transfer
244 methods for transferring leaf-level SIF simulations to top of canopy, and parameter optimization.
245 Further details on (a) photosynthetic structural formulation and parameter choice, (b)

https://doi.org/10.5194/bg-2019-508
Preprint. Discussion started: 3 February 2020

246 representation of leaf level processes important to SIF (k_N and ϕ_P), and (c) leaf-to-canopy scaling
247 approach (SIF_{canopy}) are provided in Sections 2.3.2 and 2.3.3.

248 *2.3.2 Photosynthesis Models*

249 All TBM-SIF models in this manuscript used enzyme-kinetic models to simulate leaf assimilation
250 rate (gross photosynthesis) as limited by the efficiency of photosynthetic enzyme system, the
251 amount of PAR captured by leaf chlorophyll, and the capacity of leaves to utilize end products of
252 photosynthesis (Farquhar et al., 1980; Collatz et al., 1991, 1992; Sellers et al., 1996). However,
253 there are important differences in the representation of (a) stomatal conductance that couples
254 carbon/water cycles, and (b) limiting factors on carbon assimilation due to leaf physiology
255 (maximum carboxylation capacity, Vcmax), radiation (APAR or fAPAR), canopy structure (LAI, leaf
256 angle distribution), and stress (water supply and demand, temperature), that affect plant
257 physiological processes and canopy radiative transfer. The underlying stomatal conductance
258 models in the TBMs analyzed here are represented by the Ball-Berry family of empirical models
259 rooted in the leaf gas exchange equation but with different representations of atmospheric
260 demand (relative humidity or vapor pressure deficit), including the Ball-Berry model (Ball et al.,
261 1987), the Ball-Berry-Leuning model (Leuning, 1995), the Yin-Stuik model (Yin and Struik, 2009),
262 and the Medlyn model (Medlyn et al., 2011). These structural and parametric differences also
263 influence calculated values such as the degree of light saturation (Section 2.3.3), which influence
264 both the fluorescence and quantum yield as used by the fluorescence models. Differences in
265 stomatal conductance, canopy type / radiation scheme, stress, Vcmax, and LAI are summarized
266 in Table 1.

267 *2.3.3 Fluorescence Modeling Approach*

268 Following the general approach described in Lee et al. (2015) and van der Tol et al. (2014), the
269 flux of total leaf-level emitted fluorescence, SIF_{leaf}, can be diagnosed using a light use efficiency
270 framework analogous to the expression for photosynthesis (Monteith et al., 1972),

271 $$SIF_{leaf} = fAPAR * PAR * \phi_F$$

272 $$= APAR * \phi_F \qquad \textit{Equation 1}$$

https://doi.org/10.5194/bg-2019-508
Preprint. Discussion started: 3 February 2020

where *PAR* and *fAPAR* are defined in Section 2.2.1 but measured at leaf level, and ϕ_F is the quantum yield of fluorescence, representing the number of photons emitted by fluorescence per absorbed photon. We note that photosystems I and II (PS1 and PSII, respectively) contribute to leaf level fluorescence but only PSII is considered in models analyzed here (with the exception of ORCHIDEE, Section 2.3.4.2). ϕ_F is estimated as follows:

$$\phi_F = \frac{k_F}{k_F+k_D+k_N}(1-\phi_P) \qquad \textit{Equation 2}$$

where *k* represents the rate coefficients for the different pathways for the transfer of energy from excited chlorophyll (k_F = fluorescence, k_D = heat dissipation, and k_N = non-photochemical quenching, or NPQ), and ϕ_P is the quantum yield of electron transport (see Section 2.3.2). k_F is typically set to a constant value (0.05) in models following van der Tol et al (2014). k_D is also typically set to a constant value of 0.95, or temperature corrected in some cases (e.g., ORCHIDEE, CLM4.5, CLM5.0). k_N has a substantial and variable impact on energy partitioning at diurnal and seasonal scales which varies as a function of light saturation (e.g., Raczka et al., 2019; Porcar-Castell et al., 2011). Once leaf level emissions are known, an approach is needed estimate the total TOC fluorescence flux (SIF_{canopy}) for comparison to Photospec data. Leaf and canopy level fluorescence modeling is described in more detail in Section 2.3.3.1 and 2.3.3.2 below.

2.3.3.1 Leaf level SIF emission

The 'quantum yield' approach has been used to in SIF models to characterize the fraction of photons that are used for PQ, NPQ, or re-emitted as fluorescence (van der Tol 2014). It is important to note, that this does not translate into the actual amount of SIF emission leaving the leaf, but is used as an approximation. TBM-SIF models typically represent ϕ_P using lake model formalism, which assumes large connectivity between photosynthetic units (Genty et al., 1989; van der Tol et al., 2014). ϕ_P is expressed in terms of the degree of light saturation (*x*), derived from the native photosynthesis module of the parent TBM and represents the balance between actual and potential electron transport rates, and the maximum photochemical yield under dark-acclimated conditions (ϕ_{Pmax}), which is derived from the fluorescence model and defined in terms of rate coefficients in Eq 2.

https://doi.org/10.5194/bg-2019-508
Preprint. Discussion started: 3 February 2020

300 ϕ_N accounts for the ability of plants to dissipate excess energy as heat via NPQ through the
301 regulation of xanthophyll cycle pigments (Demmig-Adams and Adams, 2006). NPQ can be
302 represented as a sum of reversible (k_R) and sustain (k_S) components ($k_N = k_R + k_S$). k_R accounts for
303 the relatively fast (diurnal), reversible NPQ response to light. k_S accounts for the relatively slow
304 (seasonal), sustained NPQ response to light and other environmental factors. With the exception
305 of CLM4.5, models do not typically account for k_S.

306 A significant challenge in fluorescence models is to find an appropriate relationship between k_N
307 and the degree of light saturation (x). The TBM-SIF models represent k_N through an approach
308 similar to the one used in SCOPE, which uses a parametric model of k_N derived from PAM
309 fluorometry measurements (van der Tol et al., 2014).

310 NPQ models can be classified as stressed (drought) and unstressed relative to water availability
311 depending on the dataset from which empirical fits are derived. The unstressed model is ideal
312 for irrigated systems such as crops, and the stressed model is more appropriate for water limited
313 ecosystems such as Niwot Ridge. We examine each of these models using drought and unstressed
314 models from van der Tol (2014), and a drought-based model from Flexas et al. (2002). These
315 models use different empirical fits but are otherwise identical. In general, k_N increases more
316 rapidly with APAR (light saturation), and ramps up to a higher level, in the drought-based model
317 compared to the unstressed model. Additionally, some models provide unique improvements
318 such as dependence on environmental conditions (e.g., water stress vs no water stress in
319 ORCHIDEE), and equations for reversible and sustained NPQ to represent the different time
320 scales (minutes to seasonal) at which NPQ regulation occurs (e.g., CLM4.5) influenced by
321 pigmentation changes in the leaf.

322 *2.3.3.2 Leaf-to-Canopy scaling*

323 The TBM-SIFs produce leaf-level fluorescence which needs to be converted to canopy-level
324 fluorescence (SIF_{canopy}) to be directly compared to PhotoSpec and satellite observations. Leaf- to
325 canopy- level conversion of SIF requires a representation of canopy radiative transfer, which in
326 general is too computationally expensive to include within the TBMs in this study, that are
327 designed for global scale application. Therefore, most TBMs analyzed here account for canopy

https://doi.org/10.5194/bg-2019-508
Preprint. Discussion started: 3 February 2020

radiative transfer of SIF using some representation of SCOPE (van der tol 2009a,b). The most commonly used approach is to run independent simulations of SIF from SCOPE to create an empirical conversion factor (κ_{740}) between leaf and canopy level SIF that is a function of Vcmax (Lee et al., 2015). This conversion factor accounts for integration over the fluorescence emission spectrum, observation angle, and unit conversion. Model variations of this empirical approach, as well additional approaches utilizing the full SCOPE model and a SCOPE emulator, are summarized below and in Table 1.

2.3.4 TBM-SIF Models

Here we provide a brief description of individual TBM-SIF models and within model experiments. We point out key differences in modeling of photosynthesis, fluorescence, and leaf-to-canopy scaling.

2.3.4.1 BETHY

The Biosphere Energy Transfer HydrologY (BETHY) model is the land surface component of the Carbon Cycle Data Assimilation System (CCDAS) developed to ingest a range of observational data for estimating GPP at global scale (Rayner et al., 2005; Kaminski et al., 2013; Koffi et al., 2012; Anav et al., 2015). Koffi et al. (2015) was the first to combine a process-based model of SIF with a global TBM. The native canopy radiative transfer and photosynthesis schemes of BETHY were effectively replaced with corresponding schemes and fluorescence model from SCOPE (Koffi et al., 2015), thus enabling spatially explicit simulation of GPP and SIF as a function of plant function type. This model was extended to include a module for prognostic leaf growth (Norton et al., 2018) and more recently adapted with a formal optimization algorithm for assimilating spaceborne SIF data (Norton et al., 2019). It has been updated for this study to accept hourly meteorological forcing. BETHY-SCOPE, denoted here as BETHY, remains the first and only global TBM-SIF model to simulate vertically integrated (1-D) fluorescence radiative transfer and energy balance.

We include three experiments to examine the impact of calibrating the k_N model against PAM fluorometry data to different species: (1) *BETHY-exp1* is adapted to unstressed cotton species (van der Tol et al., 2014), (2) *BETHY-exp2* is adapted to drought stressed Mediterranean species

https://doi.org/10.5194/bg-2019-508
Preprint. Discussion started: 3 February 2020

356 (i.e., vineyard in controlled environment subjected to drought) including higher temperature
357 correction (Flexas et al., 2002; van der Tol et al., 2014), (3) *BETHY-exp3* is adapted to drought
358 stressed Mediterranean species (Flexas et al., 2002).

359 We further leverage SCOPE enabled SIF modeling in BETHY (*BETHY-exp3* specifically) to examine
360 (a) leaf and canopy level SIF and quenching under sunlit and shaded leaves, and (b) SIF emissions
361 at the top of canopy (SIF_{canopy}) versus the average emission within the canopy (SIF_{ave}), which
362 accounts for the average emission from sunlit and shaded leaves. The latter analysis facilitates
363 comparison to PhotoSpec, which observes the entire canopy.

364 An important caveat in the analysis of BETHY simulations is that, at the time of this writing, the
365 prescribed met forcing at NR1 is only available for 2015. While this degrades comparison to
366 diurnal and synoptic variation observed by PhotoSpec in 2017, we find that analysis of
367 magnitude, light sensitivities, and within model experiments still provides useful insight for
368 interpretation of other TBM-SIFs, and future modeling requirements in general.

369 *2.3.4.2 ORCHIDEE*

370 The Organizing Carbon and Hydrology In Dynamic Ecosystems (ORCHIDEE) model (Krinner et al.,
371 2005) is the land surface component of the Earth System Model of Institut Pierre-Simon Laplace
372 IPSL-CM, (Dufresne et al., 2013) involved in recent exercises of the Coupled Model
373 Intercomparison Project (CMIP) established by the World Climate Research Programme
374 (https://www.wcrp-climate.org/wgcm-cmip). Recently a mechanistic SIF observation operator
375 was developed for ORCHIDEE to simulate the regulation of photosystem II ϕ_F at the leaf level
376 using a novel parameterization of NPQ as a function of temperature, PAR, and normalized ϕ_P. It
377 emulates the radiative transfer of SIF to the top of the canopy using a parametric simplification
378 of SCOPE. The details of the SIF modelling approach are provided in Bacour et al. (2019).

379 We include three experiments to examine the impact of water stress and parameter optimization
380 (using OCO-2 SIF, see Section 2.4): (1) *ORCHIDEE-exp1* is the standard configuration with default
381 parameters, (2) *ORCHIDEE-exp2* is the same as *ORCHIDEE-exp1* with two key differences (a) water
382 stress is applied to stomatal conductance, mesophyll conductance and to the photosynthetic

https://doi.org/10.5194/bg-2019-508
Preprint. Discussion started: 3 February 2020

383 capacity, and (b) the tree height (12 m instead of 15 m) was set specifically for the NR1 site, (3)
384 *ORCHIDEE-exp3* is the same as *ORCHIDEE-exp1* but includes OCO-2 optimized parameters.

385 *2.3.4.3 BEPS*

386 The Boreal Ecosystem Product Simulator (BEPS) is an enzyme kinetic two-leaf model for
387 simulating carbon and water cycles for different plant functional types (Chen et al., 1999; Liu et
388 al., 2003). BEPS uses a modified Ball-Berry stomatal conductance model (Leuning et al., 1995)
389 and semi-analytical canopy radiative transfer. The canopy architecture is well considered in BEPS
390 model, which has not only remote-sensed LAI but also the global map of the foliage clumping
391 index. The fluorescence emission at the leaf level follows the approach of Lee et al (2015). SIF
392 emission for sunlit and shaded leaves are separately simulated based on illumination and canopy
393 geometry in BEPS. In addition, multiple scattering SIF is also simulated to account for the
394 scattering process within the canopy. The scaling of leaf-level fluorescence emission to the
395 canopy is based on a novel scheme for single-layer models which accounts for canopy scattering
396 and extinction from sunlit and shaded leaves (Qiu et al., 2019). This scaling scheme is an effective
397 approach to simulate the radiative transfer of SIF for a given canopy structure. We include two
398 experiments similar to *BETHY-exp1/2* in the calibration of the k_N model against unstressed vs
399 stressed species (*BEPS-exp1* and *BEPS-exp2*, respectively).

400 *2.3.4.4 CLM4.5*

401 The Community Land Model version 4.5 (CLM4.5) provides a description of the biogeochemical
402 profile spanning from the sub-surface bedrock to the top of the vegetation canopy. The
403 fluorescence sub-model follows Raczka et al. (2019), in which the degree of light saturation is
404 calculated from the potential and actual electron transport rate as determined from the
405 photosynthesis model described above. ϕ_f is formulated as described in Equation 2 and ϕ_P is
406 formulated as a function of the maximum ϕ_P under dark acclimated conditions and the degree
407 of light saturation. CLM4.5 uses independent site-level SCOPE simulations that match the
408 observed canopy characteristics and observed GPP at Niwot Ridge to calculate a leaf to canopy
409 level conversion factor (κ_{740}) for estimating SIF_{canopy}. In CLM4.5, κ_{740} is fitted to the modeled
410 SCOPE data as a function of solar zenith angle (and implicitly Vcmax).

https://doi.org/10.5194/bg-2019-508
Preprint. Discussion started: 3 February 2020

411 Similar to Raczka et al. (2019), here we examine three separate approaches to parameterize k_N.
412 *CLM4.5-exp1* only considers reversible NPQ (k_R), such that, $k_N = k_R$, and the relationship
413 between k_R and the degree of light saturation is fitted to PAM fluorometry data based on
414 Mediterranean shrubs (Flexas et al., 2002; Galmes et al., 2007). *CLM4.5-exp2* parameterizes k_R
415 with PAM fluorometry from a Scots Pine forest (Porcar-Castell et al., 2011), and defines the rate
416 coefficient in terms of both a reversible and sustained component ($k_N = k_R + k_S$). It has been
417 found that sustained NPQ is important for cold climate evergreen conifer forests such as Niwot
418 Ridge (Miguez et al., 2015; Magney et al., 2019b), and Raczka et al. (2019) found that
419 representing both components provided improved simulations of seasonal SIF. *CLM4.5-exp3* is
420 similar to CLM4.5-exp3 but includes a seasonally varying representation of k_R. All model
421 experiments use hand-tuned parameters specific to US-NR1 (Raczka et al., 2016).

422 *2.3.4.5 CLM5.0*

423 CLM version 5.0 (CLM5.0) is similar to CLM4.5 with respect to the implementation of the
424 fluorescence sub-model, yet includes several important updates to the representation of
425 photosynthesis from CLM4.5, including a prognostic calculation of Vcmax based upon leaf
426 nitrogen and environmental conditions, revised nitrogen limitation scheme, Medlyn stomatal
427 conductance model, and plant hydraulic water stress (Kennedy et al., 2019). To represent NPQ
428 we use a single approach for k_N (see *CLM4.5-exp1*), but examine three approaches for estimating
429 κ_{740}: (1) *CLM5.0-exp1* uses κ_{740} as function of Vcmax following Lee et al (2015), (2) *CLM5.0-exp2*
430 follows the approach of *CLM4.5*, and (3) *CLM5.0-exp3* adapts the approach proposed by Zeng et
431 al. (2019) that estimates the fraction of total emitted SIF escaping the canopy by combining near-
432 infrared reflectance of vegetation (NIR_V) and fPAR.

433 *2.3.4.6 SIB3*

434 The Simple Biosphere Model version 3 (SIB3) involves the use of explicit biophysical mechanisms
435 to directly calculate carbon assimilation by photosynthesis (Baker et al., 2003; 2008). SiB3
436 includes prognostic calculation of temperature, moisture, and trace gases in the canopy air space,
437 but requires prescription of most structural properties including LAI. We examine two
438 approaches for prescribing LAI: (1) *SIB3-exp1* using values prescribed from MODIS, and (2) *SIB3-*

https://doi.org/10.5194/bg-2019-508
Preprint. Discussion started: 3 February 2020

exp2 uses values observed at the study site (4.0 m^2 m^{-2}). In general, the fluorescence sub-model follows the approach of Lee et al. (2015) except that k_N is adapted to drought stressed species following van der Tol et al (2014).

2.3.4.7 SIB4

SIB4 (Haynes et al., 2019a,b) shares many similarities to SIB3 with respect to functional aspects of photosynthesis and fluorescence, however, SIB4 uses prognostic rather than prescribed phenology and LAI.

2.4 Data Assimilation

Details of the data assimilation protocols for BETHY and ORCHIDEE are provided in Norton et al. (2018) and Bacour et al. (2019), respectively. For the two models, an ensemble of parameters related to photosynthesis (including optimal Vcmax) and phenology were optimized for several plant functional types. Note that none of the assimilated pixels encompass the location of the US-NR1 tower. Also, in ORCHIDEE, the study site is treated as boreal needleleaf evergreen (ENF); as such, the *ORCHIDEE-exp3* simulations in this study are based on parameters optimized against OCO-2 SIF data using an ensemble of worldwide ENF pixels. Note that for BETHY, each experiment uses the same set of optimized parameters whereas in ORCHIDEE the SIF simulations are performed separately for the standard parameters (*ORCHIDEE-exp1/exp2*) and optimized parameters (*ORCHIDEE-exp3*), thus providing a test of sensitivity to parameter optimization as discussed below.

2.5 Illumination Conditions

In order to gain insight into how SIF emissions and quantum yields vary with illumination, we further analyze Photospec and a subset of models with respect to (a) changes in incoming light and (b) self-shading within the canopy, respectively. For PhotoSpec, we analyze changes in canopy average SIF and SIF_{rel} under conditions of predominantly direct versus diffuse PAR, using the 0.5 threshold to distinguish between the two conditions (Section 2.2.2). For models we focus on emissions from sunlit vs shaded leaves. We analyze leaf- versus canopy-level SIF emissions (SIF_{leaf} and SIF_{canopy}) in *CLM4.5-exp3*, and leaf-level quantum yields (ϕ_f, ϕ_p, ϕ_N) in *BETHY-exp3*. We further compare predictions of quantum yield at the top-of-canopy to canopy averages in

https://doi.org/10.5194/bg-2019-508
Preprint. Discussion started: 3 February 2020

BETHY-exp3. The motivation here is that top-of-canopy leaves see most of the sunlight, and thus should have different yields compared to shade adapted leaves lower in the canopy. This also provides a more direct comparison for PhotoSpec.

2.6 Modeling Protocol

Models are run for the period 2000-2018 (except BETHY, 2015 only) using identical, hourly, gap-filled meteorological observations. The primary hourly output fields analyzed are the top-of-canopy SIF (SIF_{canopy} @ 740 nm), GPP, ϕ_f, ϕ_p, and APAR. Model-observation comparisons are made for absolute and relative SIF, GPP, SIF_{yield} (SIF_{canopy}/APAR) and GPP_{yield} (GPP/APAR), sunlit versus shaded canopies (*CLM4.5-exp3* and *BETHY-exp3)*, and TOC versus canopy average SIF (SIF_{canopy} versus SIF_{ave}, respectively, from *BETHY*-exp3). Quantum yields and within model experiments provide context to understand canopy integrated results. We focus our analysis on 8 am – 4 pm local time from July-August 2017 for comparison to available PhotoSpec and APAR data.

Models are controlled for meteorological forcing (meteorological data described in Burns et al., 2015) but other factors such as spin-up, land surface characteristics, parameter tuning, and model state, are not controlled for and are treated separately according to each model's protocol. For example, CLM4.5 is better suited than others in prescribing observed vegetation characteristics at the study site. Three BETHY experiment and one ORCHIDEE experiment (*ORCHIDEE-exp3*) were preliminary optimized by assimilating independent Orbiting Carbon Observatory 2 (OCO-2) SIF data at the global scale (Section 2.4). We emphasize that our point here is not to identify the best model but to identify common patterns in model behavior through normalized SIF and deviation from observed behavior to identify areas requiring the most attention.

The results are organized around two parallel themes. The first theme addresses four key processes driving canopy-level fluorescence: (1) incoming illumination, (2) energy partitioning on incoming light between photochemistry, fluorescence, and NPQ, and (3) leaf-to-canopy emitted SIF, including linearity of yields at leaf and canopy scale. The second theme addresses sensitivity of these processes to environmental conditions at diurnal and synoptic scales. Here, synoptic

https://doi.org/10.5194/bg-2019-508
Preprint. Discussion started: 3 February 2020

scale refers to the impact of day-to-day changes in weather, including two storm events which brought sustained cool, wet, and cloudy conditions from July 22-31 and then from August 6-10.

Section 3: Results

Incoming Illumination

Two key features dominate observed APAR variability: afternoon depression (Fig 2A) and reduction during two summer storms (Fig 2D). Both features are captured by models. More generally, models capture synoptic variability with high correlation (r > 0.8) and low across model spread (σ = 10%). The exception is BETHY, which is simulated outside our observation year (2015). High model fidelity is expected given that observed PAR is prescribed, and it is promising that models show a consistent response to changes in illumination. The primary shortcoming is a systematic high bias in APAR magnitude (129%), with most models exceeding the upper range of observed APAR (as determined from the six within canopy PAR sensors, Fig S2), and high model spread. These errors are likely related to differences in predicted fAPAR. In the case of ORCHIDEE, high APAR is expected due to the big leaf assumption where all eaves are considered as opaque and fully absorbing.

Canopy Photosynthesis

Observed GPP shows a broad peak from mid-morning to early afternoon (~9 am – 1 pm local), followed by slight decrease until 4 pm (Fig 2B), consistent with afternoon cooling and reduced light availability (Fig 1B-D). The two month period under investigation is relatively flat with generally weak day-to-day variability (σ = 17%), but modest correlation with APAR (r = 0.61, Fig 2E). Some models capture the afternoon GPP depression, but all models strongly underestimate its magnitude, apparently independent of stomatal conductance formulation or more explicit accounting for plant hydraulic water stress such as in CLM5.0. Models are mostly uncorrelated with observed GPP at synoptic scale (*r* ranges from -0.2 to 0.36, highest value in SiB4), high biases, and show increased spread (in predicted magnitude) relative to APAR (143% +/- 23%).

While observed GPP_{yield} is mostly stable over the diurnal cycle, most models (except BEPS) show a distinct midday minimum (Fig 3A). Half of the models show a similar midday minimum in photochemical quantum yield (ϕ_P, Fig 4A), with the other half either increasing or decreasing in

https://doi.org/10.5194/bg-2019-508
Preprint. Discussion started: 3 February 2020


Biogeosciences Discussions Open Access EGU

523 the afternoon (CLM5.0 and SiB3/SiB4, respectively). The midday dip in yield is likely associated
524 with reduced photosynthetic efficiency at high light levels, as demonstrated by reductions in GPP,
525 GPP_{yield}, ϕ_P with APAR (Fig 5A, C, E).

526 Observed GPP_{yield} shows significant structure at synoptic temporal scale (Fig 3C), most notably
527 increased yield during the cool/rainy period (reduced heat and water stress), and decreased yield
528 in mid- to late- August (increased heat and water stress following the cooling pattern). In contrast
529 to predicted GPP, models show high fidelity in capturing the magnitude and variability of GPP_{yield}
530 at synoptic scale (*r* ranges from 0.35 – 0.69, highest values in *CLM4.5* and *CLM5.0*). Individual
531 models are self-consistent in their predictions of GPP_{yield} and ϕ_P at synoptic scale (r = 0.592 –
532 0.935) except for SiB3/SiB4 (r < 0.1, Fig 4B).

533 *Canopy Fluorescence*

534 Observed SIF_{canopy} is strongly correlated with observed APAR at diurnal and synoptic scale (r =
535 0.77), with common features including afternoon depression and reduction during rainy periods
536 (Fig 2C & 2F). Observed PAR also feeds into the fluorescence sub-model and, unlike GPP, strongly
537 correlates with SIF_{canopy} at synoptic scale (*r* ranges from 0.58 to 0.92, highest values in *ORCHIDEE*).
538 However, we find a persistent positive model bias in SIF_{canopy} (170% +/- 45%) consistent with, but
539 not proportional in magnitude to, the APAR bias. We note that models are especially
540 oversensitive to APAR at high light levels (Fig 5D).

541 We investigate the high bias in SIF_{canopy} in more detail using *BETHY-exp3* and *CLM4.5-exp3*.
542 Specifically, we examine leaf and canopy level SIF and quenching under sunlit and shaded leaves.
543 Analysis of quantum yields in *BETHY-exp3* shows a reversal in the fractional amounts of absorbed
544 energy going to SIF and PQ vs NPQ in low- vs high-light conditions that is consistent with leaf level
545 data and theory (Porcar-Castell et al., 2014). More specifically, *BETHY-exp3* predicts low ϕ_F and
546 ϕ_P and high ϕ_N in sunlit leaves relative to shaded leaves, with more energy going to fluorescence
547 and photochemistry than to NPQ in shaded leaves, and more energy going to (shed off by) NPQ
548 in sunlit leaves (Fig S5). Likewise, total ϕ_F shows decreasing values with increasing APAR in
549 *BETHY-exp2/3* compared to *BETHY-exp1*, consistent with observed SIF_{yield} (Fig 5E-F), as ϕ_N ramps
550 up to higher levels in the drought parameterized Kn model. Moreover, in stark contrast to SIF_{yield}

https://doi.org/10.5194/bg-2019-508
Preprint. Discussion started: 3 February 2020

551 and SIF_{canopy}, ϕ_F does not show high values relative to other models (Fig 4D). These results point
552 to an issue in BETHY with leaf to canopy scaling in needleleaf forests.

553 Analysis of *CLM4.5-exp3* suggests several possible reasons for oversensitivity to APAR. First, we
554 focus on emissions from sunlit/shaded portions of the canopy (Fig S6). *CLM4.5-exp3* and
555 PhotoSpec both show higher SIF under "high light" conditions (sunlit leaves and direct radiation,
556 respectively) compared to "low light" conditions (shaded leaves and diffuse radiation,
557 respectively), which is promising (Fig S6 A,D). Comparing the ratio of sunlit to shaded SIF in
558 *CLM4.5-exp3* to the ratio of direct to diffuse SIF in PhotoSpec (Fig S6 B,E) shows higher ratio in
559 *CLM4.5-exp3* on average. The difference peaks in midday, when sunlit leaf area is maximized
560 (self-shading minimized) in CLM4.5 but no major difference in the amount of direct radiation,
561 and decreases with increasing sun angle (morning and afternoon) and with increasing rainfall (in
562 the afternoon on average, and during the rainy period in late July / early August), both of which
563 increase the shaded fraction. As such, accounting for view angle and different illumination
564 metrics for PhotoSpec and CLM4.5 (most comparable in morning, afternoon, and during rainy
565 days) reduces, but does not entirely remove, the positive bias in high light conditions.

566 Second, the degree of light saturation (*x*, fraction of absorbed light not used in photosynthesis)
567 is twice as high in the sunlit canopy in *CLM4.5* (Fig S7), which leads to high fluorescence efficiency
568 in sunlit leaves and low fluorescence efficiency in shaded leaves. While this produces high
569 photochemistry in shaded leaves, it contributes a small fraction of SIF to the total canopy (~20%)
570 despite higher fractions of shaded leaves (~2/3 at noon, Fig S6C) and thus sunlit leaves dominate
571 SIF_{yield} and SIF_{canopy}. Therefore, it seems likely that a model's representation of canopy structure
572 including the partitioning between sunlit/shaded canopy fraction has an important impact upon
573 canopy SIF. Biases in the sunlit/shaded will likely propagate into the simulated value of canopy
574 SIF. However, it's important to know that the observed sunlit/shaded fraction from PhotoSpec is
575 estimated as well, since it is currently no possible to determine the sun/shade fraction within
576 PhotoSpec FOV.

577 Additionally, all formulations of CLM4.5 (and most models except BETHY) show lack of decline in
578 SIF_{yield} with APAR compared to measurements of absolute SIF (Fig 5E). For CLM4.5, the
579 relationship between SIF_{yield} and APAR depends upon the relationship between degree of light

https://doi.org/10.5194/bg-2019-508
Preprint. Discussion started: 3 February 2020

saturation and reversible NPQ (Raczka et al., 2019). This suggests it is important to properly represent the NPQ response to environmental conditions when simulating SIF

While most of the model bias is reduced in SIF_{yield} (126%, mostly attributed to *BETHY*), the remaining signal, representing the dynamic response to synoptic conditions (e.g., Magney et al., 2019), is poorly represented in models (Fig 3D). Most models show zero to strongly negative correlation with observations at synoptic scale and only two models, *ORCHIDEE-exp3* and *CLM4.5-exp2*, produce positive correlation (0.58 and 0.33, respectively). These are the only two models (prescribed with 2017 met forcing) that also capture a negative relationship between SIF_{yield} and APAR (Fig 5E).

In general, predicted SIF_{yield} is stable during our short study period and is uncorrelated with GPP_{yield} (Fig 3; Fig S8). While this finding runs counter to observations of SIF_{yield}, which shows a clear response during and following the storm event and varies linearly with observed GPP_{yield} ($r = 0.40$), it is consistent with observations of SIF_{rel} (grey line in Fig 3 and Fig S8A) which like most model predictions is stable and uncorrelated with GPP_{yield}. We find it important to clarify the difference between SIF_{yield} and SIF_{rel} here, since these metrics represent different but equally important versions of reality. SIF_{yield}, estimated as the ratio between absolute canopy SIF (SIF_{canopy}) and APAR, is our best attempt to account for the effect of canopy absorbed light on the canopy integrated emission of SIF. However, factors such as observation angle, sunlit bias, and difference in footprint from APAR, necessitates our alternative calculation in SIF_{rel}. While SIF_{rel} removes model-observations differences in illumination, it confounds our interpretation of the relationship with GPP_{yield}, which is derived from APAR. As such, we provide both results to be comprehensive, but note the temporal stability associated with SIF_{rel} as the more physical interpretation of canopy yield for this short period of study.

Leaf-to-Canopy Scaling

Several methods have been proposed to transfer predicted leaf-level SIF emissions to the top of canopy. While leaf-to-canopy scaling enables efficient global scale simulation, the diversity of novel methods adds uncertainty to the canopy level estimate of SIF (in addition to aforementioned uncertainties in structure, APAR, photochemistry, fluorescence). These

https://doi.org/10.5194/bg-2019-508
Preprint. Discussion started: 3 February 2020

608 differences are evident in comparison of Figures 3 and 4, in which yields are plotted on a similar
609 scale.

610 At least at diurnal scale, there is some evidence that leaf and canopy emissions look more similar
611 for models adopting simplified empirical scaling functions (SiB3, SiB4, CLM4.5, CLM5.0, BEPS)
612 than for models that more explicitly account for radiative transfer (BETHY, ORCHIDEE). For the
613 more explicit models, the diurnal cycle of ϕ_f is out of phase with SIF_{yield}, the former of which
614 peaks in the afternoon and the latter of which peaks in the morning. This produces reasonable
615 agreement to PhotoSpec in phase and magnitude between SIF_{yield} and SIF_{rel} for ORCHIDEE, but
616 produces divergence in the magnitude of SIF_{yield} for ORCHIDEE.

617 Model performance in leaf-to-canopy scaling is summarized in Figure S8. The only two models
618 with a positive relationship between yields (Fig S8B) and between quenching terms (Fig S8C) are
619 the two models with more explicit representation of radiative transfer (i.e., ORCHIDEE and
620 BETHY). CLM4.5 is the only model with a positive relationship between yields, but not between
621 quenching terms. SiB3/SiB4 are the only models with a positive relationship between quenching
622 terms, but not between yields.

623 Finally, we note that PhotoSpec scans of leaf-level emissions are averaged and reported here as
624 canopy averages, while model output is reported at the top of the canopy, which accounts for
625 within-canopy radiative transfer, re-absorption of SIF, and shaded canopies, causing lower
626 emissions compared to the canopy average. CLM4.5, for example, shows strong attenuation of
627 SIF from leaf-level to TOC, decreasing by a factor of 2-3 at midday (Fig S7). The interpretation
628 here is that the model bias in absolute SIF may actually be higher than reported here; however,
629 we note that more quantitative information on the observed fraction of sunlit vs shaded leaves
630 and comparative top-of-canopy SIF values for the same canopy elements are needed (to account
631 for off-nadir SIF viewing) for more accurate determination of scaling between observed canopy
632 and top-of-canopy SIF.

633 *Within Model Experiments*

634 In most cases, within model experiments produce improvements in some metrics and
635 degradation across others (performance change is quantified by reporting correlation values in

https://doi.org/10.5194/bg-2019-508
Preprint. Discussion started: 3 February 2020

brackets). An important and unexpected result of this study is the impact of different levels of tuning to observations on our predictions. While this work represents a snapshot of the state-of-the-art in site-level TBM-SIF modeling, and we have taken great care to control for environmental conditions (most important being illumination), an important overall takeaway is for future model comparisons to make additional efforts to control for initial conditions and vegetation state.

The most basic example is tuning of LAI in SiB3. LAI, as prescribed by MODIS for *SiB3-exp1* (~1.5), is on the low end for a subalpine evergreen forest, and consequently produces negative biases in APAR, GPP, SIF and SIF_{yield}. When prescribed according to tower observations in *SiB3-exp2* (~4.0), the biases become positive (albeit on the lower end of the model ensemble), but produces degraded variation at synoptic scale for GPP (0.39 vs 0.19), SIF (0.87 vs .71) and SIF_{yield} (0.09 vs -0.32).

Experiments in CLM4.5 comprise a higher level of hand tuning of vegetation structural and functional characteristics. Parameter tuning was imposed to match vegetation structure with site level measurements and consequently CLM4.5 produces overall low bias in yields. With respect to synoptic variation, NPQ experiments, tuned against the measured air temperature and a representative evergreen forest, produce improvements at synoptic scale for GPP (-0.01 vs 0.16), SIF (0.59 vs 0.86), and GPP_{yield} (0.05 vs 0.63), but degradation in SIF_{yield} (0.32 vs -0.25). Likewise, NPQ experiments in BETHY based on species information (calibration of K_N against PAM fluorescence in stressed vs unstressed systems) shows improvement in the SIF_{yield}-APAR relationship for drought stressed models (*BETHY-exp1* vs *BETHY-exp2/3*).

Experiments with ORCHIDEE demonstrate that errors in model parameters (such as Vcmax, LAImax, leaf age, or SLA) contribute to SIF and GPP uncertainty but can be alleviated by assimilation of OCO-2 SIF retrievals (*ORCH-exp1/2* vs *ORCH-exp3*). Model optimization of parameters improves the functional link between SIF and GPP, thus reducing biases in APAR, GPP, and SIF_{yield}, and improving synoptic variation in SIF_{yield} (-0.04 vs 0.58).

Section 4. Discussion

https://doi.org/10.5194/bg-2019-508
Preprint. Discussion started: 3 February 2020


Biogeosciences Discussions Open Access EGU

663 This study represents a first attempt to evaluate a controlled ensemble of TBM-SIF models
664 against canopy integrated SIF observations to identify and attribute model-observation
665 mismatches related to errors in canopy absorption of sunlight, photosynthesis, fluorescence, and
666 leaf-to-canopy radiative transfer of fluorescence.

667 Different models match some observed parameters better than others (with respect to APAR and
668 yield), but no model gets both APAR and SIF_{yield} magnitude and/or sensitivities close to the
669 observations. For example, BEPS closely matches the magnitude of APAR (Fig 2A), and BETHY
670 captures the decline in SIF_{yield} with APAR for NPQ quenching based on stressed species (Fig 5E),
671 but both models overestimate observed yield by a factor of 2, hence SIF is overestimated (Fig 2).
672 CLM4.5 correctly captures the diurnal SIF_{yield} change, but overestimate APAR; in this case, SIF and
673 SIF_{yield} are overestimated. Importantly, models diverge strongly from each other and from
674 observations in the magnitude of SIF_{yield} and its decline with APAR (Fig 5E), partially reflecting
675 model variability in ϕ_f (Fig 5F), but in general show a characteristic pattern of weak SIF_{yield} decline
676 with APAR. GPP_{yield} shows higher agreement between models and with observations (Fig 5B),
677 despite divergent ϕ_P (Fig 5C), which could be indication that the primary uncertainty is due to
678 the representation of fluorescence and not the photosynthesis model.

679 Consequently, we find a strong linear and positive relationship between observed SIF_{yield} and
680 GPP_{yield} for absolute SIF, which is underestimated on average by models (Fig 6A-B). In contrast,
681 models show quite strong positive relationships between ϕ_f and ϕ_P (Fig 6C). Our study highlights
682 an apparent challenge for models in transferring leaf level processes to canopy scale, and
683 consequently, linking the proper canopy mechanistic SIF-GPP relationship at the leaf level.

684 The mismatch between multi-model simulations and tower-based observations of SIF and GPP
685 at hourly and daily scales can be summarized as symptoms of five main factors: (1) PhotoSpec
686 scan strategy, (2) radiative transfer of incoming PAR and impact on APAR and sunlit/shaded
687 fraction, (3) representation of photosynthesis and sensitivity to water limitation especially during
688 afternoon conditions, (4) representation of fluorescence and sensitivity to reversible NPQ
689 response at Niwot Ridge, and (5) radiative transfer of fluorescence from leaf to canopy. Several
690 persistent biases falling under these broad categories are discussed below.

https://doi.org/10.5194/bg-2019-508
Preprint. Discussion started: 3 February 2020

691 **Apples to Apples Comparison**.

692 PhotoSpec is unique in its ability to scan entire canopies for signals that are largely hidden from
693 nadir-oriented instruments. However, this creates unique challenges for interpretation of data
694 and comparison to models. For example, the diurnal cycle of observed SIF is highly sensitive to
695 view angle. PhotoSpec was set up in 2017 to scan back-and-forth between northwest and
696 northeast view angles, but the instrument was slightly biased to the northwest, causing a low
697 phase angle in the morning (more aligned with rising sun) and increased phase angle in the
698 afternoon (more opposed to setting sun). As such, PhotoSpec observed predominantly
699 illuminated canopies in the morning and shaded canopies in the afternoon (i.e., more shaded
700 fraction), leading to the late morning peak in reflected radiance (Fig S3).

701 Moreover, Photospec scans specific locations at the top of the canopy from near nadir to view
702 angles closer to the horizon (see Fig. S8 in Magney et al., 2019b), while models are currently
703 configured to simulate top of canopy emission and simulated here as nadir viewing. The question
704 becomes whether to retain nadir only data and sacrifice signal-to-noise, or to average over all
705 elevation angles and risk aliasing view angle effects. This study, partly motivated by high
706 agreement of canopy integrated SIF with spaceborne data from OCO-2 and TROPOMI (Magney
707 et al., 2019b; Parazoo et al., 2019), has chosen the latter approach but with an attempt to
708 minimize scan angle effects in SIF_{rel}. However, it is worth noting that swath sensors such as
709 GOME-2 show high sensitivity to viewing angle especially under increasing illumination angles
710 (Kohler et al., 2018; Joiner et al., in review). View angle effects are likely to be especially acute
711 for PhotoSpec in the morning and afternoon with increasing anisotropy and changes in the
712 illuminated field of view with sun and view angle. Other tower SIF instruments with a wide FOV
713 (i.e. FluoSpec2; Yang et al., 2018) may more appropriately represent the TOC SIF emission, but
714 also have difficulty disentangling the sunlit/shaded canopy components.

715 It is critical that model evaluation relative to measured SIF data and data assimilation studies
716 properly account for the specificities of the instrument (viewing of the instrument, spectral band,
717 time of the overpass for space-borne instruments), the representation of canopy emission, and
718 correct observations for directional variations in SIF relative to observation geometry. Although
719 normalizing SIF by reflected radiance partially alleviates scan angle effects, this highlights the

https://doi.org/10.5194/bg-2019-508
Preprint. Discussion started: 3 February 2020

need for models to get canopy structure, radiative transfer, and sunlit/shaded fraction correct, which feed all the way through to SIF and GPP. Further ground-based investigations of SIF anisotropy, sunlit/shade fraction, and vertical distribution (within canopy, canopy integrated, and top of canopy) with PhotoSpec may help to inform models on the physical aspects of the signal. Despite the issues we highlight in comparing observations to models, the potentially more interesting and important story here is with respect to model-model comparisons, which reveals wide divergence in response to light conditions and other factors, as discussed below.

TBM SIF is too sensitive to APAR.

Our results indicate a spectrum of SIF responses to APAR: TBMs are usually far too sensitive to APAR, observations of absolute SIF are less sensitive, and observations of relative SIF are least sensitive. The fact that relative SIF is the least sensitive is telling, as it reduces sensitivity to APAR and reveals a strong SIF response to changes in photochemical quenching. SIF models appear especially sensitive to sunlit leaves. In CLM4.5, SIF emissions from the sunlit portion of the canopy are a factor of 5 higher than emissions from shaded leaves, despite twice as fewer leaves in the sunlit canopy (Fig S6C). In CLM4.5, the combination of higher than average ϕ_f (Fig 5F) with higher fluorescence efficiency in the sunlit portion of the canopy, produce an increase in the magnitude and sensitivity to sunlit fraction, thus contributing to the high bias (factor of 3 higher than observed) and strong diurnal cycle (2-fold increase from morning to midday).

Linearity of SIF and GPP yields.

Observations show a positive but not significant linear relationship between SIF_{yield} and GPP_{yield} (Fig 6A, r = 0.40) at our study site. This is likely due to the short time period investigated here where there is relatively little change in SIF_{yield} and GPP_{yield} during peak summer. Only 3 of 7 models show a significant (r > 0.35) linear and positive slope (r > 0.35; ORCH-exp3, CLM4.5-exp3, and BETHY-exp3) between SIF_{yield} and GPP_{yield}, while 5 models (except CLM5.0) show a significant positive slope between quantum yields (ϕ_f and ϕ_p, Fig 6C). These regression plots of quantum yields, in turn, help explain the observed linearity of SIF_{yield} vs. GPP_{yield}: At least in the case of Niwot Ridge, model (and presumably observed) ϕ_p stays within high light "NPQ-Phase" conditions, and generally doesn't exceed the range in which decoupling of ϕ_f and ϕ_p (ϕ_p > 0.6)

https://doi.org/10.5194/bg-2019-508
Preprint. Discussion started: 3 February 2020

748 in low light "PQ-Phase' conditions occurs (Porcar-Castell et al., 2014, cf Fig 9). BETHY-exp3, which
749 best captures the observed relationship in the canopy between SIF_{yield} and GPP_{yield}, is also the
750 only model that also shows a decline in SIF_{yield} with APAR, as discussed below. These results are
751 likely to change when we expand the study to several years; however, the purpose of this study
752 was to provide an initial investigation into the response of modelled SIF and GPP to light during
753 peak summer.

754 **Insufficient decline in SIF_{yield} with APAR.**

755 In general, models show an insufficient decline in SIF_{yield} with APAR, when compared to observed
756 SIF_{yield} (Fig 5E). All models except SiB3 and SiB4 show some decline, with BETHY showing the best
757 agreement in slope magnitude. BETHY is the only model with full radiative transfer but this does
758 not appear to have a substantial impact on SIF_{yield}, which has a similar (albeit suppressed) decline
759 with APAR as ϕ_f (Fig 5F). Within model experiments show little to no sensitivity of SIF_{yield} or ϕ_f
760 decline with APAR to water stress (e.g., ORCHIDEE) or prescribed LAI (e.g., SiB3), but high
761 sensitivity to the formulation of NPQ with respect to species calibration (e.g., BETHY) and
762 reversibility (e.g., CLM4.5).

763 Three CLM4.5 experiments demonstrate sensitivity to representation of NPQ variability at diurnal
764 and seasonal scales. The first simulation using the default NPQ parameterization from SCOPE
765 (*CLM4.5-exp1*, based on a 2-parameter fit to drought stressed Mediterranean species (Galmes et
766 al., 2007) produces the strongest decline in SIF_{yield}. The second simulation, which includes a site-
767 specific NPQ formulation that accounts for k_R and k_S (*CLM4.5-exp2*), produces the weakest
768 decline. The third simulation with seasonally varying k_R produces a slightly stronger decline. An
769 important point for this formulation is that k_R is constrained by PAM fluorometry data at Hyytiala
770 (Scot Pine) and does not account for high light saturation values and summer drought conditions
771 that may be more typical of lower latitude sites such as Niwot Ridge. This could indicate that
772 parameterizing k_R based upon similar PFTs may not be sufficient to properly characterize the NPQ
773 response for lower latitude sites such as Niwot Ridge.

774 Similar results are found in experiments with BETHY comparing stressed (drought) and
775 unstressed (relative to water availability) NPQ models at NR1 but controlling for k_R (constant in

https://doi.org/10.5194/bg-2019-508
Preprint. Discussion started: 3 February 2020

time in both cases, stronger negative SIF_{yield} response to APAR in stressed model). In the unstressed models of CLM4.5 and BETHY, the NPQ response to APAR becomes too low, causing an oversensitivity of SIF to APAR and thus high SIF bias. The strongly regulated NPQ response of the drought-based model enables more non-photochemical quenching at high light levels in stressed ecosystems compared to typical unstressed plants. While this k_{NPQ} model was developed using drought-stressed plants, similar up-regulation of NPQ is expected to occur under any condition where photosynthesis is limited and available excitation energy is high (e.g. cold temperatures and high light, Sveshnikov et al., 2006, doi: 10.1093/treephys/26.3.325). Our results thus emphasize the need for careful implementation of NPQ dynamics for simulating and assimilating SIF in different light and stress environments (Raczka et al., 2019; Norton et al., 2019).

Data assimilation reduces high bias. Assimilation of OCO-2 SIF in ORCHIDEE brings the magnitude of both GPP and SIF in closer agreement with observations. This improvement is driven by decreases in leaf photosynthetic capacity (Vcmax, LAImax, leaf age, SLA, Bacour et al., 2019), which decreases the magnitude (but not shape) of APAR closer to observed values (Fig 2), and leads to improvements in GPP_{yield} and SIF_{yield} (Fig 3). Nevertheless, after the assimilation there are still disagreements in SIF_{yield} vs GPP_{yield} relative to the measured quantities (Fig 6). For diurnal and synoptic cycles, the assimilation effectively acts to scale the magnitude of SIF, GPP and APAR (and related yields), but it does little to alter variability. Although data assimilation (i.e. calibrating model parameters) is critical to improving modelled SIF and GPP, this should be done in conjunction with improvements in the model formulation (as summarized in Section 5), otherwise the estimated model parameters can be sub-optimal to compensate for the lack of missing processes.

5. Conclusions/Recommendations

Our results reveal systematic biases across TBM-SIF models affecting leaf-to-canopy simulations of APAR, GPP, and SIF. This highlights key areas where observing strategies and model formulations can be improved:

https://doi.org/10.5194/bg-2019-508
Preprint. Discussion started: 3 February 2020

1) Radiative transfer of incoming and absorbed PAR. The representation of incoming radiative transfer produces positive biases in APAR that leads to positive biases in GPP, both of which occur regardless of time of day. This is influenced by characterization of the canopy, leaf orientation and clumping, biochemical content, canopy layers, and leaf area, which dictates the sunlit/shaded fractions of the canopy. Furthermore, the combination of high APAR bias in models and high uncertainty in observed APAR highlights a need for more accurate and representative in situ measurements of APAR within the FOV of SIF observations and footprint of eddy covariance data.

2) Water stress impacts on photosynthesis. The underlying photosynthetic models fail to simulate the magnitude of depression of observed GPP in the afternoon, regardless of stomatal-conductance or water stress formulation. This likely results from the inability to account for afternoon water stress to properly restrict stomatal conductance and hence GPP and SIF. Additional effort is needed to characterize SIF and GPP sensitivity to increased atmospheric demand and/or reduced soil moisture.

3) Leaf Mechanism for Energy Partitioning. We provide evidence that many models fail to capture the correct reversible NPQ response to light saturation, leading to biases in SIF_{yield} during high light conditions and especially with increasing moisture limitation at the end of summer. Further investigation using models such as BETHY and CLM is needed to better characterize sensitivity of NPQ formulations to PFT and environmental conditions.

4) Radiative transfer of SIF. SIF is emitted from the leaf level (sunlit shaded fractions of leaf level) and then is transferred to the top of canopy as a function of canopy structure (leaf geometry, canopy layers, leaf area). Despite high disagreement of BETHY-SCOPE with respect to the simulation of APAR and SIF magnitude, we recommend site level simulations using a similar framework where a radiative transfer model is coupled to a terrestrial biosphere model for more detailed investigation of sensitivity to canopy characteristics.

5) Observation strategy. The PhotoSpec scan strategy enables direct measurement of SIF emission at leaf-to-canopy scale, but requires off-nadir view angles that lead to changing fractions of sunlit and shaded canopies throughout the day as a function of sun angle. Further

https://doi.org/10.5194/bg-2019-508
Preprint. Discussion started: 3 February 2020

work could be done using tower mounted instruments with a wider FOV that more accurately represent top of canopy emissions for comparison to model simulations, and to classify emissions from shaded vs sunlit canopies.

Acknowledgements

The US-NR1 AmeriFlux site is supported by the U.S. DOE, Office of Science through the AmeriFlux Management Project (AMP) at Lawrence Berkeley National Laboratory under Award Number 7094866. BMR was supported by the NASA CMS Project (award NNX16AP33G) and the US Department of Energy's Office of Science, Terrestrial Ecosystem Science Program (awards DE-SC0010624 and DE-SC0010625). CESM (CLM4.5 and CLM5.0) is sponsored by the National Science Foundation and the U.S. Department of Energy. ORCHIDEE is supported by CNES-TOSCA under the FluOR and ECOFLUO projects. ITB was supported by NASA contract 80NSSC18K1312. We would like to thank the W.M. Keck Institute for Space Studies and internal funds from the Jet Propulsion Laboratory for support of the field measurements at Niwot Ridge (http://www.kiss.caltech.edu/study/photosynthesis/technology.html). A portion of this research was carried out at JPL, California Institute of Technology, under contract with NASA. This work was supported in part by the NASA Earth Science Division MEaSUREs program (grant 17-MEASURES-0032) and ABoVE program (18-TE18-0062). Copyright 2019. All rights reserved.

https://doi.org/10.5194/bg-2019-508
Preprint. Discussion started: 3 February 2020

References

Anav, A., Friedlingstein, P., Beer, C., Ciais, P., Harper, A., Jones, C., Murray-Tortarola, G., Papale, D., Parazoo, N.C., Peylin, P., and Piao, S.: Spatiotemporal patterns of terrestrial gross primary production: A review, Reviews of Geophysics, 53(3), 785-818, https://doi.org/10.1002/2015RG000483, 2015.

Albert, L. P., Keenan, T. F., Burns, S. P., Huxman, T. E., and Monson, R. K.: Climate controls over ecosystem metabolism: insights from a fifteen-year inductive artificial neural network synthesis for a subalpine forest, Oecologia, 184(1), 25–41. https://doi.org/10.1007/s00442-017-3853-0, 2017

Bacour, C., Maignan, F., MacBean, N., Porcar-Castell, A., Flexas, J., Frankenberg, C., Peylin, P., Chevallier, F., Vuichard, N., and Bastrikov, V.: Improving estimates of Gross Primary Productivity by assimilating solar-induced fluorescence satellite retrievals in a terrestrial biosphere model using a process-based SIF model, Journal of Geophysical Research: Biogeosciences, 124(11), 3281-3306, 2019.

Baker, I.T., Prihodko, L., Denning, A.S., Goulden, M., Millller, S., and da Rocha, H.: Seasonal Drought Stress in the Amazon: Reconciling Models and Observations, J.Geophys. Res., 113, G00B01, doi:10.1029/2007JG000644, 2008.

Baker, I.T., A.S. Denning, N. Hanan, L. Prihodko, P.-L. Vidale, K. Davis and P. Bakwin: Simulated and observed fluxes of sensible and latent heat and CO2 at the WLEF-TV Tower using SiB2.5, Glob. Change Biol., 9, 1262-1277, 2003.

Ball, J. T., Woodrow, I. E., and Berry, J. A.: A model predicting stomatal conductance and its contribution to the control of photosynthesis under different environmental conditions, Progress in photosynthesis research, Springer, Dordrecht, 221-224, 1987.

Burns, S. P., Blanken, P. D., Turnipseed, A. A., Hu, J., and Monson, R. K.: The influence of warm-season precipitation on the diel cycle of the surface energy balance and carbon dioxide at a Colorado subalpine forest site, Biogeosciences, 12, 7349–7377, 2015.

Chen, J. M., Liu, J., Cihlar, J., and Goulden, M. L.: Daily canopy photosynthesis model through temporal and spatial scaling for remote sensing applications, Ecological Modelling, 124(2–3), 99–119, 1999.

Demmig-Adams, B., Cohu, C. M., Muller, O., and Adams, W. W.: Modulation of photosynthetic energy conversion efficiency in nature: from seconds to seasons, Photosynthesis Research, 113(1–3), 75–88. https://doi.org/10.1007/s11120-012-9761-6, 2012.

Dufresne, J.-L., Foujols, M.-A., Denvil, S., Caubel, A., Marti, O., Aumont, O., Balkanski, Y., Bekki, S., Bellenger, H., Benshila, R., and Bony, S.: Climate change projections using the IPSL-CM5

https://doi.org/10.5194/bg-2019-508
Preprint. Discussion started: 3 February 2020

883 Earth System Model: from CMIP3 to CMIP5, Climate Dynamics, 40(9–10), 2123–2165,
884 2013.

885 Flexas, J., Escalona, J. M., Evain, S., Gulías, J., Moya, I., Osmond, C. B., and Medrano, H.: Steady-
886 state chlorophyll fluorescence (Fs) measurements as a tool to follow variations of net CO2
887 assimilation and stomatal conductance during water-stress in C3 plants. Physiologia
888 Plantarum, 114(2), 231–240. https://doi.org/10.1034/j.1399-3054.2002.1140209.x, 2002.

889 Friedlingstein, P., Meinshausen, M., Arora, V. K., Jones, C. D., Anav, A., Liddicoat, S. K., and
890 Knutti, R.: Uncertainties in CMIP5 climate projections due to carbon cycle feedbacks,
891 Journal of Climate, 27(2), 511–526, 2014.

892 Galmés, J., Flexas, J., Savé, R., and Medrano, H.: Water relations and stomatal characteristics of
893 Mediterranean plants with different growth forms and leaf habits: responses to water
894 stress and recovery, Plant and Soil, 290(1–2), 139–155, 2007.

895 Gastellu-Etchegorry, J. P., Malenovský, Z., Duran Gomez, N., Meynier, J., Lauret, N., Yin, T., Qi,
896 J., Guilleux, J., Chavanon, E., Cook, B., Morton, D.: Simulation of chlorophyll fluorescence
897 for sun- and shade-adapted leaves of 3D canopies with the DART model, International
898 Geoscience and Remote Sensing Symposium (IGARSS), 2018-July, 5995–5998.
899 https://doi.org/10.1109/IGARSS.2018.8517576, 2018.

900 Grossmann, K., Frankenberg, C., Magney, T. S., Hurlock, S. C., Seibt, U., and Stutz, J.: PhotoSpec:
901 A new instrument to measure spatially distributed red and far-red Solar-Induced
902 Chlorophyll Fluorescence, Remote Sensing of Environment, 216, 311–327.
903 https://doi.org/10.1016/j.rse.2018.07.002, 2018.

904 Gu, L., Han, J., Wood, J. D., Chang, C. Y., and Sun, Y.: Sun-induced Chl fluorescence and its
905 importance for biophysical modeling of photosynthesis based on light reactions, New
906 Phytologist, nph.15796. https://doi.org/10.1111/nph.15796, 2019.

907 Gu, L., Wood, J. D., Chang, C. Y. Y., Sun, Y., and Riggs, J. S.: Advancing Terrestrial Ecosystem
908 Science With a Novel Automated Measurement System for Sun-Induced Chlorophyll
909 Fluorescence for Integration With Eddy Covariance Flux Networks, Journal of Geophysical
910 Research: Biogeosciences, 124(1), 127–146. https://doi.org/10.1029/2018JG004742, 2019.

911 Haynes, K., Baker, I. T., Denning, S., Stöckli, R., Schaefer, K., Lokupitiya, E. Y., and Haynes, J. M.:
912 Representing grasslands using dynamic prognostic phenology based on biological growth
913 stages: 1. Implementation in the Simple Biosphere Model (SiB4), Journal of Advances in
914 Modeling Earth Systems, 11. https://doi.org/10.1029/ 2018MS001540, 2019a.

915 Haynes, K. D., Baker, I. T., Denning, A. S., Wolf, S., Wohlfahrt, G., Kiely, G., Minaya, R. C., and
916 Haynes, J. M.: Representing grasslands using dynamic prognostic phenology based on
917 biological growth stages: 2. Carbon cycling, Journal of Advances in Modeling Earth
918 Systems, 11. https:// doi.org/10.1029/2018MS001541, 2019b.

https://doi.org/10.5194/bg-2019-508
Preprint. Discussion started: 3 February 2020

Kaminski, T., Knorr, W., Schürmann, G., Scholze, M., Rayner, P. J., Zaehle, S., Blessing, S., Dorigo, W., Gayler, V., Giering, R., and Gobron, N.: The BETHY/JSBACH carbon cycle data assimilation system: Experiences and challenges, Journal of Geophysical Research: Biogeosciences, 118(4), 1414–1426, 2013.

Kennedy, D., Swenson, S., Oleson, K. W., Lawrence, D. M., Fisher, R., Lola da Costa, A. C., and Gentine, P.: Implementing plant hydraulics in the community land model, version 5, Journal of Advances in Modeling Earth Systems, 11(2), 485-513, 2019.

Koffi, E. N., Rayner, P. J., Scholze, M., and Beer, C.: Atmospheric constraints on gross primary productivity and net ecosystem productivity: Results from a carbon-cycle data assimilation system, Global Biogeochemical Cycles, 26(1), https://doi.org/10.1029/2010GB003900, 2012.

Koffi, E. N., Rayner, P. J., Norton, A. J., Frankenberg, C., and Scholze, M.: Investigating the usefulness of satellite-derived fluorescence data in inferring gross primary productivity within the carbon cycle data assimilation system, Biogeosciences, 12(13), 4067–4084, 2015.

Krinner, G., Viovy, N., de Noblet-Ducoudré, N., Ogée, J., Polcher, J., Friedlingstein, P., Ciais, P., Sitch, S., and Prentice, I. C.: A dynamic global vegetation model for studies of the coupled atmosphere-biosphere system, Global Biogeochemical Cycles, 19(1), 2005.

Lee, J.-E., Berry, J. A., van der Tol, C., Yang, X., Guanter, L., Damm, A., Baker, I., and Frankenberg, C.: Simulations of chlorophyll fluorescence incorporated into the Community Land Model version 4, Global change biology, 21 (9), 3469-3477, 2015.

Leuning R.: A critical appraisal of a combined stomatal-photosynthesis model for C_3 plants, Plant Cell Environ, **18**: 339–357, 1995.

Li, Z., Zhang, Q., Li, J., Yang, X., Wu, Y., Zhang, Z., Wang, S., Wang, H., and Zhang, Y.: Solar-induced chlorophyll fluorescence and its link to canopy photosynthesis in maize from continuous ground measurements, Remote Sensing of Environment, 236, 111420, 2020.

Liu, J., Chen, J. M., and Cihlar, J.: Mapping evapotranspiration based on remote sensing: An application to Canada's landmass, Water Resources Research, 39(7), 2003.

Liu, W., Atherton, J., Mõttus, M., Gastellu-Etchegorry, J. P., Malenovský, Z., Raumonen, P., et al.: Simulating solar-induced chlorophyll fluorescence in a boreal forest stand reconstructed from terrestrial laser scanning measurements, Remote Sensing of Environment, (July 2018), 111274, https://doi.org/10.1016/j.rse.2019.111274, 2019.

Medlyn, B.E., Duursma, R.A., Eamus, D., Ellsworth, D.S., Prentice, I.C., Barton, C.V.M., Crous, K.Y., De Angelis, P., Freeman, M., and Wingate, L.: Reconciling the optimal and empirical approaches to modelling stomatal conductance, Global Change Biology, 17: 2134–2144. doi:10.1111/j.1365-2486.2010.02375.x, 2011.

https://doi.org/10.5194/bg-2019-508
Preprint. Discussion started: 3 February 2020

955 Magney, T. S., Frankenberg, C., Fisher, J. B., Sun, Y., North, G. B., and Davis, T. S.: Connecting
956 active to passive fluorescence with photosynthesis : a method for evaluating remote
957 sensing measurements of Chl fluorescence, New Phytologist, 215(4), 1594-1608,
958 https://doi.org/10.1111/nph.14662, 2017.

959 Magney, T. S., Frankenberg, C., Köhler, P., North, G., Davis, T. S., Dold, C., Dutta, D., Fisher, J. B.,
960 Grossmann, K., Harrington, A., Hatfield, J.: Disentangling Changes in the Spectral Shape of
961 Chlorophyll Fluorescence: Implications for Remote Sensing of Photosynthesis, Journal of
962 Geophysical Research: Biogeosciences, 124(6), 1491-1507,
963 https://doi.org/10.1029/2019JG005029, 2019a.

964 Magney, T. S., Bowling, D. R., Logan, B., Grossmann, K., Stutz, J., and Blanken, P.: Mechanistic
965 evidence for tracking the seasonality of photosynthesis with solar-induced fluorescence,
966 Proceedings of the National Academy of Sciences, 116 (24), 11640-11645,
967 https://doi.org/10.1073/pnas.1900278116, 2019b.

968 Miguez, F., Fernández-Marin, B., Becerril, J. M., and Garcia-Plazaola, J. I.: Activation of
969 photoprotective winter photoinhibition in plants from different environments: a literature
970 compilation and meta-analysis, Physiologia Plantarum, 155(4), 414–423, 2015.

971 Mohammed, G. H., Colombo, R., Middleton, E. M., Rascher, U., van der Tol, C., Nedbal, L.,
972 Goulan, Y., Perez-Priego, O., Damm, A., Meroni, M. and Joiner, J.: Remote sensing of solar-
973 induced chlorophyll fluorescence (SIF) in vegetation: 50 years of progress, Remote Sensing
974 of Environment, 231, 111177, https://doi.org/10.1016/j.rse.2019.04.03, 2019.

975 Monteith, J. L.: Solar Radiation and Productivity in Tropical Ecosystems, J. Appl. Ecol., 9, 747–
976 766, https://doi.org/10.2307/2401901, 1972.

977 Norton, A. J., Rayner, P. J., Koffi, E. N., and Scholze, M.: Assimilating solar-induced chlorophyll
978 fluorescence into the terrestrial biosphere model BETHY-SCOPE v1. 0: model description
979 and information content, Geoscientific Model Development, 11(4), 1517–1536, 2018.

980 Norton, A. J., Rayner, P. J., Koffi, E. N., Scholze, M., Silver, J. D., and Wan, Y.-P.: Estimating global
981 gross primary productivity using chlorophyll fluorescence and a data assimilation system
982 with the BETHY-SCOPE model, Biogeosciences, 16(15), 3069-3093, 2019.

983 Porcar-Castell, A.: A high-resolution portrait of the annual dynamics of photochemical and non-
984 photochemical quenching in needles of Pinus sylvestris, Physiologia Plantarum, 143(2),
985 139–153, https://doi.org/10.1111/j.1399-3054.2011.01488.x, 2011.

986 Qiu, B., Chen, J. M., Ju, W., Zhang, Q., and Zhang, Y.: Simulating emission and scattering of
987 solar-induced chlorophyll fluorescence at far-red band in global vegetation with different
988 canopy structures, Remote Sensing of Environment, 111373, 2019.

989 Raczka, B., Porcar-Castell, A., Magney, T., Lee, J. E., Köhler, P., Frankenberg, C., Grossman, K.,
990 Logan, B.A., Stutz, J., Blanken, P. D., Burns, S. P., Duarte, H., Yang, X., Lin, J. C., and Bowling,

https://doi.org/10.5194/bg-2019-508
Preprint. Discussion started: 3 February 2020

991 D. R.: Sustained nonphotochemical quenching shapes the seasonal pattern of solar-
992 induced fluorescence at a high-elevation evergreen forest, Journal of Geophysical
993 Research: Biogeosciences, 124, 2005–2020, https://doi.org/10.1029/2018JG004883, 2019.

994 Rayner, P. J., Scholze, M., Knorr, W., Kaminski, T., Giering, R., and Widmann, H.: Two decades of
995 terrestrial carbon fluxes from a carbon cycle data assimilation system (CCDAS), Global
996 Biogeochemical Cycles, 19(2), 2005.

997 Schreiber, U., Schliwa, U., and Bilger, W.: Continuous recording of photochemical and non-
998 photochemical chlorophyll fluorescence quenching with a new type of modulation
999 fluorometer, Photosynthesis Research, 10, 51–62, 1986.

1000 Sellers, P. J., Randall, D. A., Collatz, G. J., Berry, J. A., Field, C. B., Dazlich, D. A., Zhang, C., Collelo,
1001 G. D., and Bounoua, L.: A revised land surface parameterization (SiB2) for atmospheric
1002 GCMs. Part I: Model formulation, Journal of Climate, 9(4), 676–70, 1996.

1003 Van Der Tol, C., Berry, J. A., Campbell, P. K. E., and Rascher, U.: Models of fluorescence and
1004 photosynthesis for interpreting measurements of solar-induced chlorophyll fluorescence,
1005 Journal of Geophysical Research: Biogeosciences, 119(12), 2312–2327.
1006 https://doi.org/10.1002/2014JG002713, 2014.

1007 Yang, P., and van der Tol, C.: Linking canopy scattering of far-red sun-induced chlorophyll
1008 fluorescence with reflectance, Remote Sensing of Environment, 209(May), 456–467.
1009 https://doi.org/10.1016/j.rse.2018.02.029, 2018.

1010 Yin, X., and Struik, P. C.: C3 and C4 photosynthesis models: an overview from the perspective of
1011 crop modelling, NJAS-Wageningen Journal of Life Sciences, 57(1), 27-38, 2009.

1012 Zhang, Y., Guanter, L., Berry, J. A., van der Tol, C., Yang, X., Tang, J., and Zhang, F.: Model-based
1013 analysis of the relationship between sun-induced chlorophyll fluorescence and gross
1014 primary production for remote sensing applications, Remote Sensing of Environment, 187,
1015 145–155, 2016.

1016 Zhang, Q., Zhang, X., Li, Z., Wu, Y., and Zhang, Y: Comparison of Bi-Hemispherical and
1017 Hemispherical-Conical Configurations for In Situ Measurements of Solar-Induced
1018 Chlorophyll Fluorescence, Remote Sensing, 11, 2642, 2019.

1019

https://doi.org/10.5194/bg-2019-508
Preprint. Discussion started: 3 February 2020

1020 **Figures**

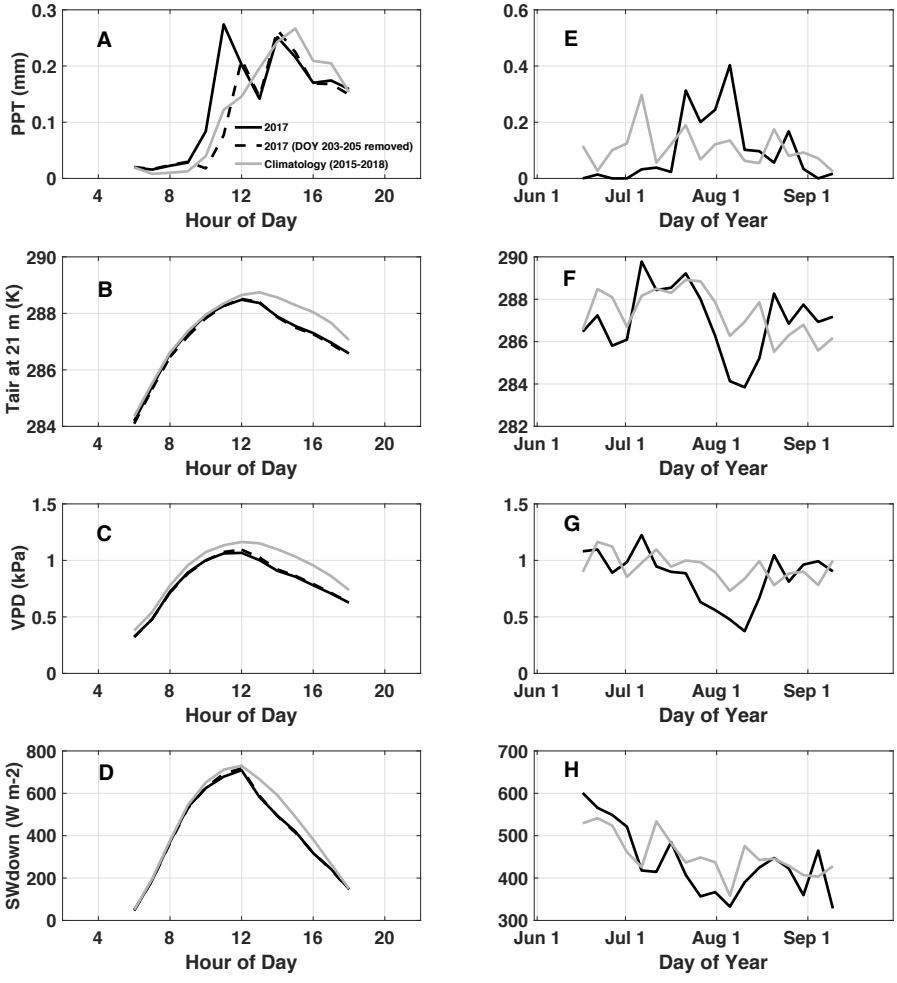

1021

1022 **Figure 1**. Observed diurnal (A-D) and synoptic (E-H) precipitation (PPT), air temperature at 21 m
1023 (Tair), vapor pressure deficit (VPD), and downwelling shortwave (SWdown). Diurnal cycles are
1024 averaged over July-August, 2017. Synoptic cycles are plotted as 5-day averages from June 15 –
1025 Sep 15. Data from 2017 is shown in black and climatology (2015-2018) in grey. Typically, peak
1026 rainfall occurs in the afternoon at this site (A). A substantial rain event which occurred from DOY
1027 203-205 is removed from the 2017 average to show the impact on diurnal variability and to
1028 demonstrate the dominance of the afternoon monsoon upon diurnal precipitation in summer.

https://doi.org/10.5194/bg-2019-508
Preprint. Discussion started: 3 February 2020

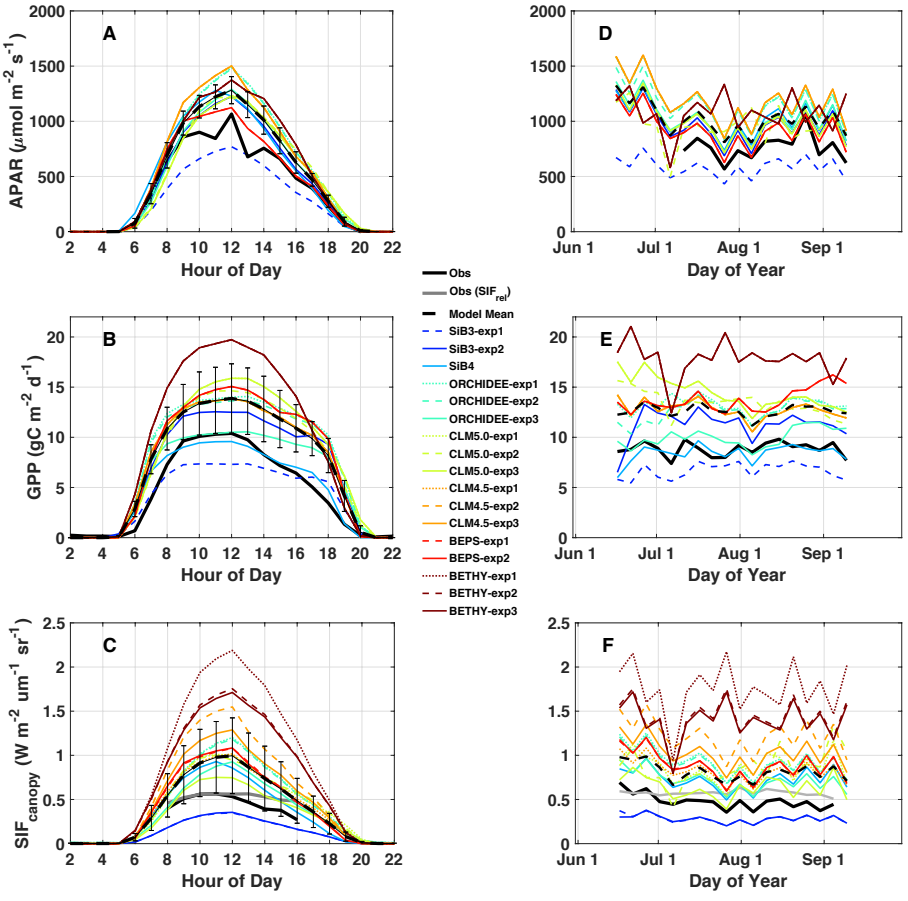

Figure 2. Observed and simulated diurnal cycles of APAR, GPP and SIF. Diurnal cycles (A-C) are averaged over July-August, 2017. Synoptic cycles (E-F) are plotted as 5-day averages from June 15 – Sep 15. Observations are shown in black, with relative SIF (SIF_{canopy} / far red reflected radiance) included in (C, F) in grey. The across model average (dashed black) represents the average of "best-case" model scenarios (solid lines; SiB3-exp2, SiB4, ORCHIDEE-exp3, CLM5.0-exp3, CLM4.5-exp3, BEPS-exp2, BETHY-exp3) with uncertainty bars indicating the across model 1 sigma uncertainty.

https://doi.org/10.5194/bg-2019-508
Preprint. Discussion started: 3 February 2020

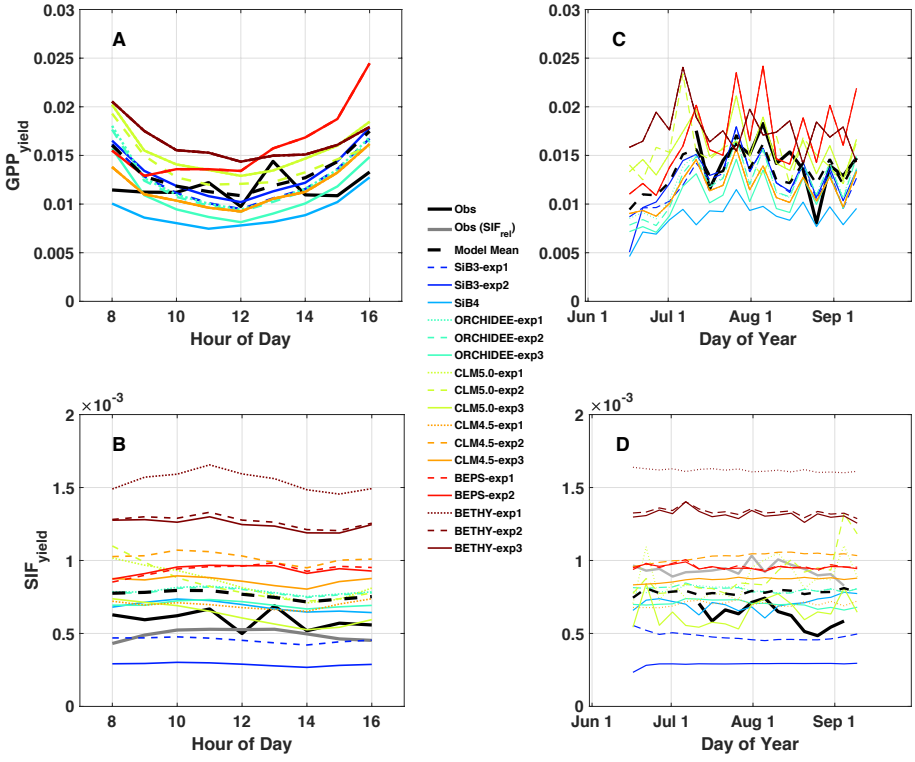

1037

1038 **Figure 3**. Same as Figure 2 except for SIF_{yield} and GPP_{yield}. Here, SIF_{yield} = SIF_{canopy} / APAR, and

1039 GPP_{yield} = GPP / APAR.

1040

https://doi.org/10.5194/bg-2019-508
Preprint. Discussion started: 3 February 2020

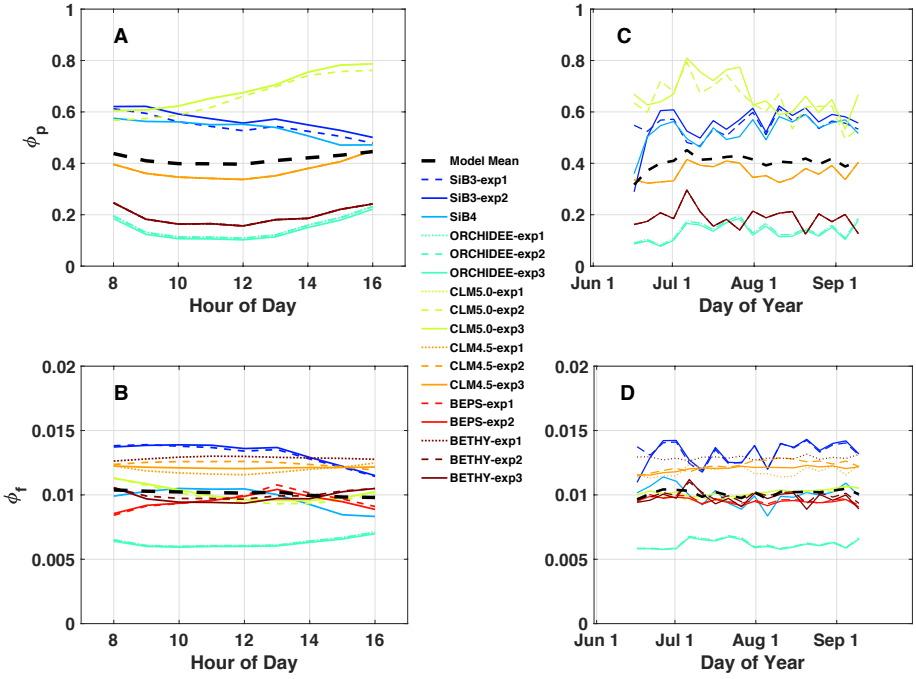

Figure 4. Same as Figure 2, except for quantum yield of fluorescence (ϕ_F) and photochemistry (ϕ_P).

https://doi.org/10.5194/bg-2019-508
Preprint. Discussion started: 3 February 2020

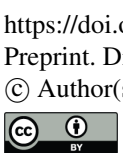

Biogeosciences
Discussions
Open Access
EGU

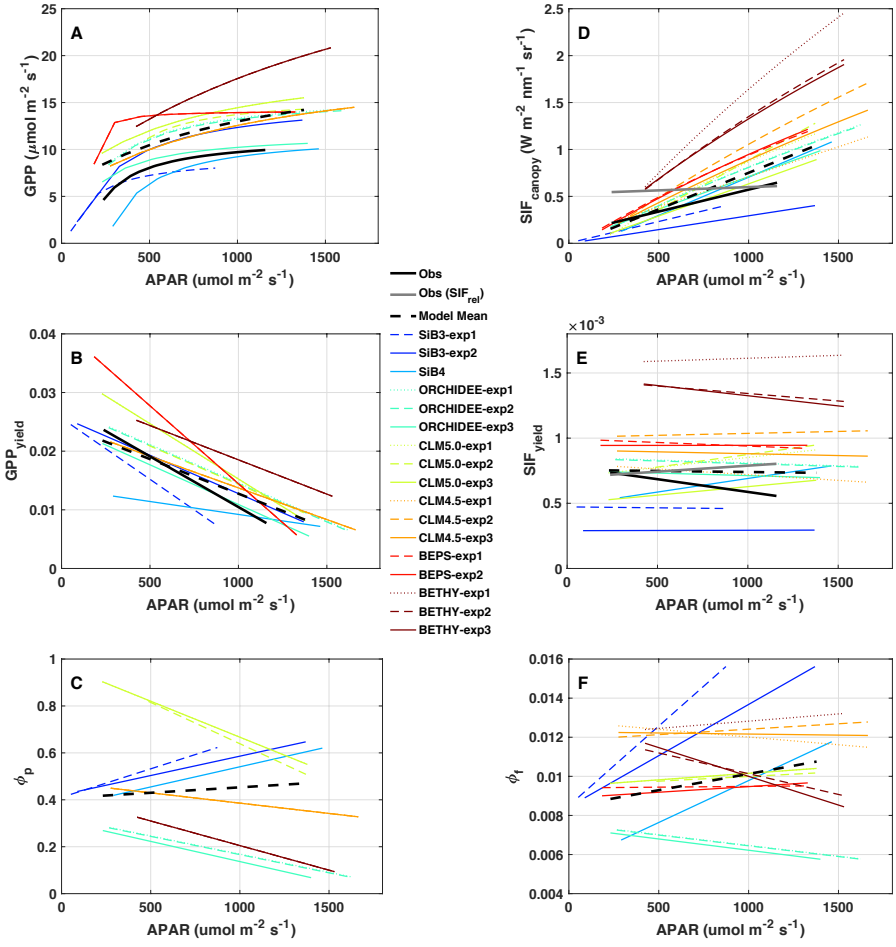

Figure 5. Observed and predicted change in GPP, SIF, and yields with APAR. Regression lines are shown for (A) GPP, (B) GPP_{yield}, (C) photochemical quantum yield (ϕ_p), (D) SIF_{canopy}, (E) SIF_{yield}, (F) fluorescence quantum yield (ϕ_f), as a function of APAR, using daily mean (8 am – 4 pm local) values over the period July-August 2017. Observations are shown in solid black, individual models and experiments in color, the across model average in dashed black. Relative SIF is shown in grey in (D) and (E).

https://doi.org/10.5194/bg-2019-508
Preprint. Discussion started: 3 February 2020

Biogeosciences Discussions Open Access EGU

Tables

Table 1. Summary of TBM-SIF models and within model experiments illustrating model components that may have led to differences in modeled SIF., These include a representation of stomatal-conductance (column 3), canopy absorption of incoming radiation (column 4), limiting factors for photosynthesis (Stress, Vcmax, LAI; columns 5-7) and SIF (k_N; column 8), leaf-to-canopy scaling of SIF (column 9), and parameter optimization (column 10). The underlined model experiment was used for model intercomparison .

Model (TBM-SIF reference)	Model Experiments	Stomatal Conductance	Canopy Type / Radiation	Stress	Vcmax	LAI	k_N	Leaf-to-Canopy Scaling	Parameter Optimization
BETHY (Norton et al., 2019)	BETHY-exp1	Ball-Berry	Multiple Layers Sunlit/Shaded = Yes Fpar/APAR = semi-analytical canopy radiative model (SCOPE, based on SAIL)	Ta and water stress	Prior is a function of Ta, then optimized against OCO-2	Prescribed (4.0 m^2 m^{-2})	Adapted to unstressed cotton species (Tol et al., 2014)	SCOPE radiative transfer. f(Ta, APAR, structure, leaf composition) via dependence of photosynthetic rate on ϕ_f	Optimized against OCO-2
	BETHY-exp2						Adapted to drought stressed Mediterranean species including high temperature correction (Tol et al., 2014; Flexas et al., 2002)		
	BETHY-exp3						Adapted to drought stressed Mediterranean species (Flexas et al., 2002)		
ORCHIDEE (Bacour et al., 2019)	ORCHIDEE-exp1	Yin-Struik	Big Leaf Model Sunlit/Shaded = No APAR = Beer-Lambert law depending on LAI and extinction factor = 0.5	Ta stress	f (leaf age, CO_2, Ta, water stress)	prognostic	Adapted to needleleaf species (Porcar-Castell et al., 2011) and unstressed Mediterranean species (Flexas, 2002), with added dependence on PAR, temperature, and ϕ_P	Parametric representation of SCOPE (v1.61) to emulate radiative transfer within canopy for PSI/II.	Default
	ORCHIDEE-exp2			Ta and water stress (Yin and Struik, 2009)					Default
	ORCHIDEE-exp3			Same as exp 1					Global ENF PFT optimized against OCO-2
BEPS (Qiu et al., 2019)	BEPS-exp1	Ball-Berry-Leuning	Single Layer Sunlit/Shaded = Yes Fpar = semi-analytical canopy radiative transfer	Soil water stress factor (ratio of measured soil available water to maximum plant available water)	Prescribed	prescribed	Adapted to water stressed Mediterranean species (Galmes et al., 2007)	Parametric representation of radiative transfer physics to account for canopy scattering effects	Default
	BEPS-exp2						Adapted to drought stressed Mediterranean species including high temperature correction (Tol et al., 2014; Flexas et al., 2002)		
CLM4.5 (Raczka et al., 2019)	CLM4.5-exp1	Ball-Berry	Single Layer Sunlit/Shaded = Yes	Ta(Vcmax); soil moisture stress uses Btran parameterization (function of column rooting profile and soil water potential)	Prescribed (calibrated against observed GPP at NR1)	Prescribed (4.0 m^2 m^{-2})	Adapted to water stressed Mediterranean species (Galmes et al., 2007)	κ_{740} = f(Vcmax, SZA), calibrated to offline SCOPE runs using prescribed canopy characteristics at NR1	Hand-tuned to NR1 (Raczka et al., 2016)
	CLM4.5-exp2						Adapted to needleleaf species (Porcar-Castell et al., 2011); Accounts for sustained NPQ (k_s) separately from reversible NPQ (k_d). k_s is calibrated to NR1 Tair. k_d is fixed in time		
	CLM4.5-exp3						same as Exp 2, but k_d is seasonal		
CLM5.0 (unpublished)	CLM5.0-exp1	Medlyn	Single Layer Sunlit/Shaded = Yes	Plant hydraulic water stress (Sperry and Love, 2015; Lawrence et al., 2019) accounting for water demand and supply	f (soil moisture, nitrogen), calibrated to NR1	Prescribed (4.0 m^2 m^{-2})	Adapted to water stressed Mediterranean species (Galmes et al., 2007)	κ_{740} = f(Vcmax), calibrated to offline SCOPE runs from Lee et al. (2015)	Default
	CLM5.0-exp2							κ_{740} = f(Vcmax, SZA), calibrated to offline SCOPE runs using prescribed canopy characteristics at NR1	
	CLM5.0-exp3							Escape ratio (f_{esc}), derived from NIRv and fPAR (Zeng et al., 2019)	
SiB3 (Baker et al., 2003, 2008) SiB4 (Haynes et al., 2019a,b)	SiB3-exp1	Ball-Berry	Single Layer Sunlit/Shaded = Yes	Downregulation by VPD, Ta, and soil moisture	f (soil moisture)	Prescribed (MODIS)	Adapted to drought stressed species (Tol et al., 2014)	κ_{740} = f(Vcmax), calibrated to offline SCOPE runs from Lee et al. (2015)	Default
	SiB3-exp2					Prescribed (4.0 m^2 m^{-2})			
	SiB4					Prognostic			